Reliability assessment of robustness for reinforced concrete moment resisting frames

RELIABILITY ASSESSMENT OF ROBUSTNESS FOR REINFORCED CONCRETE MOMENT RESISTING FRAMES

Elena Miceli[1], Diego Gino[2], Paolo Castaldo[3]

[1]Department of Structural, Geotechnical and Building Engineering (DISEG), Politecnico di Torino, Turin, Italy. (Corresponding author) E-mail: elena.miceli@polito.it

[2]Department of Structural, Geotechnical and Building Engineering (DISEG), Politecnico di Torino, Turin, Italy. E-mail: diego.gino@polito.it

[3]Department of Structural, Geotechnical and Building Engineering (DISEG), Politecnico di Torino, Turin, Italy. E-mail: paolo.castaldo@polito.it

Corresponding Author

Miceli Elena

elena.miceli@polito.it

+39 0110905305

RELIABILITY ASSESSMENT OF ROBUSTNESS FOR REINFORCED CONCRETE MOMENT RESISTING FRAMES

Elena Miceli[1], Diego Gino[2], Paolo Castaldo[3]

[1]Department of Structural, Geotechnical and Building Engineering (DISEG), Politecnico di Torino, Turin, Italy. (Corresponding author) E-mail: elena.miceli@polito.it

[2]Department of Structural, Geotechnical and Building Engineering (DISEG), Politecnico di Torino, Turin, Italy. E-mail: diego.gino@polito.it

[3]Department of Structural, Geotechnical and Building Engineering (DISEG), Politecnico di Torino, Turin, Italy. E-mail: paolo.castaldo@polito.it

ABSTRACT

A strain-based 5-step procedure is illustrated for the probabilistic robustness assessment of 2D reinforced concrete moment resisting frames. Considering the central column removal as failure scenario, this study compares three frames, including a code-conforming design (*frame 1*) and two enhanced designs (*frame 2* and *frame 3*). For the three frames, non-linear finite-element (NLFE) models have been defined including properly calibrated translational springs. By sampling from materials and loads, 300 displacement-controlled pushdown NLFE global analyses have been conducted to determine energy-based dynamic amplification factors (1.02 - 1.75). Next, 300 probabilistic static-equivalent NLFE global analyses, performed by removing the column and amplifying loads, permitted to monitor the aleatory peak strains in any material and point of the frames. This allowed to compute the failure probabilities with respect to the ultimate limit state. Robustness improvements lead to much lower failure probabilities (10^{-7} - 10^{-3}) in any element with a reduction of damage propagation.

Keywords: structural robustness; reliability assessment; reinforced concrete moment resisting frames; strain-based 5-step procedure; probabilistic static-equivalent NLFE global analyses; energy-based dynamic amplification factor.

1. INTRODUCTION

Terrible events like the terrorist attack of 2001, which caused the total collapse of the so-called Twin Towers and thousands of victims, represented a shock for the entire community, not only for the consequences due to the structural collapse of the buildings, but mostly for human losses. In the past decades, such catastrophic phenomena on strategic structures, caused by exceptional events, brought architecture, engineering and construction experts to show a growing interest towards structural robustness, especially with respect to more sustainable systems [1]-[3] as well as optimized and reliable solutions [4]-[6]. European code rules [7]-[11] have been integrated by specific sections regarding structural robustness with suggestions or general requirements. The concept of extreme actions and their consequences on a structure have been deepened by many international guidelines [12]-[17]. In this way, it has been more and more clear that risk analysis should become part of strategies for collapse prevention against low-probability high-consequence (LPHC) events to investigate both socially acceptable and technically feasible solutions [18]. In this context, effects of aging on structure lifetime [19] as well as extraordinary events of natural or anthropic origin, like

explosions, avalanches or terroristic attacks, can determine critical conditions for structural systems. The local collapse of a bearing element can trigger a chain reaction of structural element failures, eventually leading to partial or full structural collapse as well described in [20]-[22]. A particular situation, which has been deeply analysed by many authors [23]-[26], is the progressive collapse due to a sudden column loss. The study of such problem is of interest to understand the entity of the resistance reserves provided by the membrane and catenary effects [27]. Previous studies have predominantly concentrated on the theoretical quantification of structural robustness. For instance, [28] proposed a simplified tying force method, specifically designed to assess the progressive collapse performance of reinforced concrete (RC) systems. Analytical models have been developed to evaluate the ultimate bearing capacity of RC slabs in scenarios involving column loss, both for one-way and two-way RC slabs [29] as well as RC flat slabs [30]. The study in [31] introduces an analytical model highlighting the role of catenary forces under extreme lateral loading, focusing on cases where damage is localized in a single structural member without complete column loss.

Another group of studies focuses on quantitative risk analysis. In fact, the level of safety associated to LPHC events can be reliably investigated through quantitative risk analysis in probabilistic terms, since it allows to include the uncertainties affecting engineering issues [32]. For example, a sensitivity analysis is elaborated in [33] to compute the bearing capacity of different RC structural members in case of the removal of a central supporting element. Fragility analyses are performed in [34] in case of low-rise RC buildings to compute the exceedance probability of different damage states given a column loss scenario. Global variance-based sensitivity analysis is used in [35] to study the major sources of uncertainties in the response of RC structures subjected to sudden column loss. A reliability-based index of structural collapse in case of extreme events is computed in [36], for 2D linear elastic truss systems by randomly sampling loads and strengths. A probabilistic analysis of steel-concrete composite floor against progressive collapse considering uncertainties of strengths and loads in steel connections is performed by [37], concluding that using load combinations from "General Services Administration - GSA" [20] may lead to a non-conservative design. The reliability of RC frames under different column-loss scenarios is investigated in [38], obtaining failure probabilities ranging from 0.016 to 0.137 and identifying side column-loss scenario as the worst case if the presence of infill walls is not considered. The work [39] proposes a multilevel scheme to evaluate the reliability of planar RC frames obtaining system failure probabilities of 0.254 and 0.173 for inner frames considering, respectively, 6-story and 3-story office buildings.

The actual code rules do not provide any requirement of a progressive collapse risk assessment as well as associated reliability levels for buildings or bridges. Considering a reference period of 1 year for a structural system, values higher than 1 for the reliability index are recommended in [14].

This study describes a strain-based 5-step procedure for the probabilistic robustness assessment of 2D RC moment resisting (MR) frames designed in seismic area. Considering a progressive collapse scenario involving the loss of a central supporting column, three different frames are analysed: one designed according to seismic codes (i.e., *frame 1*) and two other ones (i.e., *frame 2* and *frame 3*) where the reinforcement arrangement is properly modified to achieve a more robust behaviour in terms of both bearing capacity and catenary effect, according to [40]. In detail, the *frame 2* adopts a continuous reinforcement along the beams over the supports with two additional levels of side face rebars, while the *frame 3* derives from the *frame 2* adopting the same reinforcement amount in all the floors with symmetric cross-sections to exploit a global Vierendeel behaviour. For the three entire frames, non-linear finite element (NLFE) global models have been defined in ATENA 2D including the contribution of the orthogonal structural frames by means of equivalent translational springs. Within a full probabilistic approach, for each frame, 100 random combinations have been sampled from the aleatory properties of both materials and applied loads through the Latin Hypercube Sampling (LHS) technique [41]. The aleatory properties denote the variables characterised by randomness. Specifically, eleven different random variables have been sampled regarding the concrete properties, reinforcing steel properties and concerning both permanent and variable loads according to [7]-[10],[42]-[46]. After that, three sets of 100 displacement-controlled pushdown NLFE

global analyses have been performed, by applying an increasing vertical displacement where the central supporting column had been removed. From the resulting capacity curves (i.e., displacement-reaction curves), the energetic equivalence approach [23] has been applied to compute the corresponding dynamic amplification factors (DAFs) for each one of the 300 sampled frames. These DAFs have been useful to perform 300 probabilistic static-equivalent NLFE global analyses, by removing the central supporting column and amplifying the loads on the spans close to the removed column. Successively, the peak strains monitored in both confined concrete and reinforcement in different points of the frames have been probabilistically modelled. By convolution integrals between the strain distributions with the corresponding ultimate threshold distributions, the failure probabilities with respect to the ultimate limit state (ULS) have been estimated in any structural element of the three RC MR frames. The comparison between the three RC MR frames provides reference values of the failure probabilities and shows the relevant safety advantages when robustness improvements are adopted: the failure probabilities are strongly lower in the spans close to the collapse scenario, the safety level increases in any structural element for increasing distance from the collapse event highly reducing the damage propagation.

2. RELIABILITY ASSESSMENT OF STRUCTURAL ROBUSTNESS: PROPOSED FRAMEWORK

Structural reliability means the capability of a structure or a structural member to fulfil the specified requirements during the reference lifetime, for which it has been designed [47]. The basic requirements are intended in terms of safety, serviceability, durability and robustness [11]. In order to quantify these requirements, the so-called limit states (or performance functions) are identified as the conditions beyond which the structure, or a part of it, does no longer satisfy one of its performance requirements [7],[11]. Reliability analysis represents a powerful method to deal with uncertainties in engineering design [48]. These uncertainties differ for many aspects (e.g., the nature of the structure itself, environmental conditions and applied actions) and can be distinguished between aleatory, which are related to the inherent randomness of loads and of structural properties (i.e., mechanical and geometrical), and epistemic, connected to the lack of knowledge and consequential assumptions to model the variables [49]. The measure of the reliability is the failure probability P_f with respect to the limit state function or the reliability index β [7],[11],[50]-[51]. The methods to assess the reliability can be classified in four levels [11]: full probabilistic methods (i.e., level III); probabilistic methods (i.e., level II) (e.g., FOSM (first order second moment) or FORM (first order reliability methods)); semi-probabilistic methods (i.e., level I); deterministic methods (i.e., level 0). In this work, the full-probabilistic method has been adopted together with the Latin Hypercube Sampling (LHS) technique [41], which represents a stratified sampling technique employed to generate samples of random variables with an even distribution over the corresponding domains.

Structural robustness is one of the performance requirements that a structure should guarantee when dealing with structural reliability. In general, it can be defined as the capability of a structure or a structural member to avoid disproportionate damage, with respect to an exceptional action that has caused the damage. The structural robustness can be assessed by means of a probabilistic risk analysis (PRA), based on the concept of conditional probability [14]. Considering H as the hazard, connected thus to the dangerous event, and considering LD as the local damage, the probability of structural collapse $P[C]$ can be computed [14] as follows:

$$P[C] = P[C \mid LD] \cdot P[LD \mid H] \cdot P[H] \tag{1}$$

where $P[C|LD]$ is the conditional probability of disproportionate collapse, given the local damage LD, $P[LD|H]$ denotes the conditional probability of local damage given the event H and $P[H]$ represents the occurrence probability of the event depending on its mean annual occurrence rate λ_H.

In the hypothesis to investigate the robustness of a frame after an accidental event which causes the sudden removal of a supporting column, the reliability assessment can be focused on the computation of the term $P[C|LD]$, considering that the local damage LD occurs (i.e., $P[LD|H]$ is equal to unity) if

there is the happening of the dangerous event H (e.g., gas explosion, terrorist attacks, failure at the foundation level, excessive loads, etc.) characterised by its specific mean annual rate λ_H [14],[52]. For the reliability assessment of structural robustness of a frame within the full probabilistic approach, the following strain-based 5-step procedure is followed (Fig. 1), inspired by [23],[41],[53]-[54]:

1. The aleatory properties of both structure (e.g., materials and geometry) and loads have to be sampled (e.g., through LHS method) defining N_{tot} aleatory structures (as detailed in Section 5).
2. A preliminary analysis is needed by performing displacement-controlled pushdown NLFE global simulations, where any aleatory structure is modelled without the supporting column and a progressively increasing displacement is imposed at the point where the column is removed. From these simulations, the reaction at the same point of the removed column is monitored to define the probabilistic capacity curves (i.e., displacement-reaction curves). Additional details are given in Section 6.
3. The computation of the DAFs: the dynamic amplification factor represents the increase of the structural response to a static load to reproduce the dynamic application of the same load. The energy equivalence approach can be followed, according to [23], to find the energetic equilibrium corresponding to the equivalence between the work done by the external load and the internal energy given by the structure. The approach is adopted to compute the dynamic displacement and corresponding dynamic gravitational load P_d on the probabilistic capacity curves. In this way, the DAFs can be evaluated as the ratios between the dynamic and static gravitational loads (as further described in Section 6).
4. Probabilistic static-equivalent NLFE global analyses have to be performed simulating the removal of the column and amplifying the loads of the adjacent spans in each floor through the energy-based DAFs, while the other spans are loaded with the non-amplified gravity loads. Additional features are given in Subsection 7.1.
5. The aleatory results in terms of peak strains for the different materials have to be treated in probabilistic terms to assess the reliability at structural level with respect to the ultimate limit state (ULS), given by the onset of the ultimate strains of the materials. An in-depth description is reported in Subsection 7.2.

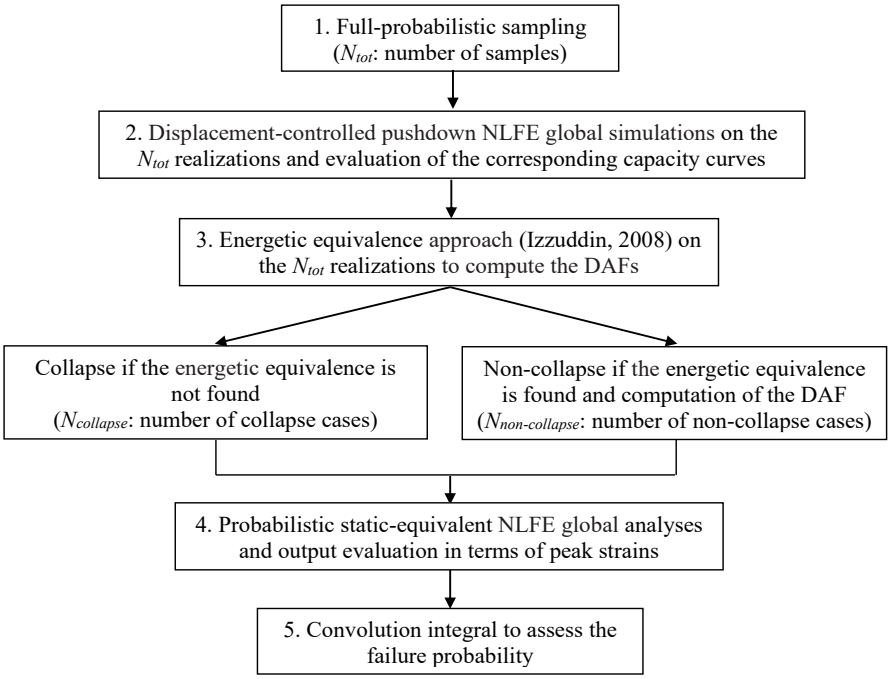

Fig. 1 Flowchart of the 5-step strain-based procedure.

This procedure ensures to take into account, in a simplified way, the dynamicity of such failure scenario avoiding the complexity of performing dynamic analyses but, at the same time, allowing to

consider both geometrical and material non-linearities within non-linear simulations of the entire structure [55]. However, it should be noted that other effects, due to dynamic features which can lead to instability phenomena, are not included.

3. DESIGN OF 2D RC MR FRAMES IN SEISMIC ZONE WITH DIFFERENT REINFORCEMENT LAYOUTS

3.1 Seismic design according to current standards: "frame 1"

The starting point of this work is to design a 2D multi-storey reinforced concrete (RC) moment resisting (MR) frame, regular in elevation and symmetric, consisting of four floors plus roof with four spans.

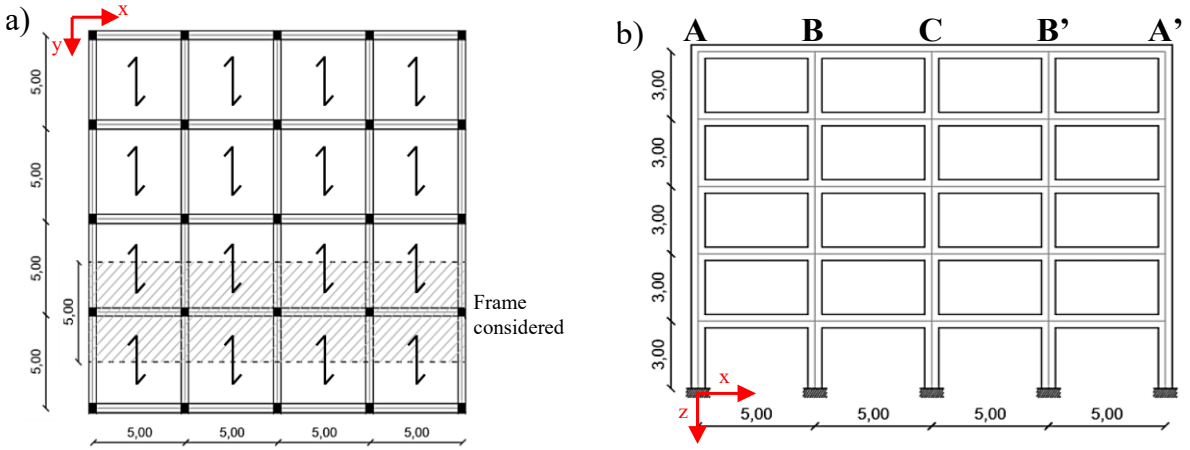

Fig. 2 Geometry of the multi-storey RC MR frame: (a) plan view with joists framework direction; (b) lateral view. Measurements in m.

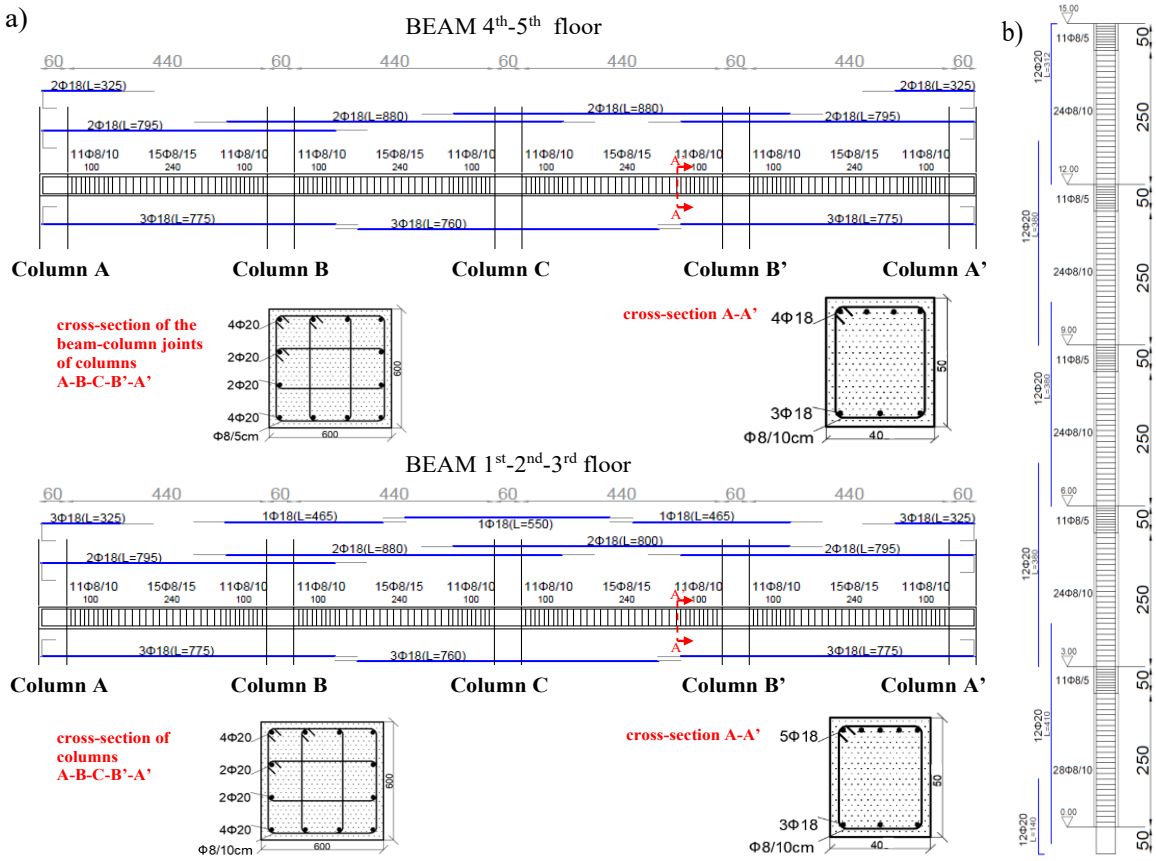

Fig. 3 Longitudinal and transverse reinforcement arrangement for: (a) beams with specific cross-sections and their positions; (b) columns and joints. Measurements in cm.

The inter-storey height is equal to 3m for all the floors, the length of all the spans is equal to 5m and the transverse effective width is equal to 5m (Fig. 2). The structure is located in L'Aquila city (Italy) and a high ductility class is assumed according to [9],[57].
As for the materials, the reinforcing bars are made of B450C steel [9]-[10], while C25/30 concrete [9]-[10] with 3.5cm of clear concrete cover is used in any structural element.
Static and modal analyses have been carried out to design the geometry together with the longitudinal and transverse reinforcement with respect to ULSs, serviceability limit states (SLSs) and the capacity design principles for seismic verifications in all the structural elements [8]-[10],[57]. Fig. 3 illustrates the reinforcement detailing obtained from the verifications: in particular, ϕ18 longitudinal bars and ϕ8 stirrups are adopted, for all the structural elements.
All the beams have dimensions of 40x50cm^2. The transversal reinforcement in the beams is made of 2-legs ϕ8 stirrups arranged with a spacing of 10cm in the dissipative zone and 15cm in the central zones of the spans, for all the floors. The transversal and longitudinal reinforcement of the beams are depicted in Fig. 3(a). The dissipative zone has a length of 100cm from the beam-column joint.
Regarding the columns, they all have 60x60cm^2 cross-sections. The longitudinal reinforcement is made of 12ϕ20 bars (located symmetrically in both directions), while the shear reinforcement is made of 4-legs ϕ8 stirrups with a spacing of 10cm, along the entire length of the structural element apart from the beam-column joints where the spacing is equal to 5cm. The transversal and longitudinal reinforcement of both the columns and joints are depicted in Fig. 3(a)-(b).

3.2 Seismic design according to robustness improvements: "frame 2" and "frame 3"

Other two frames have been designed with proper modifications in the longitudinal reinforcement arrangement to improve the response against a column removal scenario, adopting the criteria combined with the cyclic procedure proposed and investigated in [40].
The *frame 2* is characterised by the following assumptions: all the longitudinal reinforcement bars are displaced continuously along the beams, respecting the suggestions to ensure the continuity over the supports and for at least 30% of the span length in addition to the anchorage length, according to [40] and [12]-[15]. This derives from the major extension of the bending moment in the upper chord of the beams due to the column loss. It follows that the new arrangement of the longitudinal reinforcement is made of 3ϕ18 in the lower chord of all the beams of the five floors, while 5ϕ18 in the upper chord for the beams in the first three floors and 4ϕ18 for the beams in the last two floors. In addition, two levels of 2ϕ16 side face rebars (placed at around 1/3 and 2/3 of the beam height) are arranged continuously over all the beams for all the floors. The presence of the side face reinforcement bars can anticipate the catenary effect activation because they can provide an important contribution to a tension response, facilitating tie behavior [40]. It should be noted that the change of the longitudinal reinforcement arrangement within the beams needed to be verified at the ULSs and seismic verifications. Thus, the stirrup step in the dissipative area for the beams in all the floors was modified from 10cm to 7.5cm. The other structural elements remained unchanged with respect to the *frame 1* (Fig. 4(a)). This new arrangement of the *frame 2* is depicted in Fig. 4(b).
The third frame (i.e., *frame 3*) derives from the *frame 2* by applying a symmetric reinforcement between the upper and lower chord of the beams and arranging the same amount of reinforcement in the beams of the first floor (i.e., the largest one) to the beams of all the other floors. The symmetry criterion, as also suggested by [34],[40], is considered because when a loss of a load-bearing column occurs, some sections undergo to opposite bending moments in sign. Instead, the equal reinforcement criterion is followed to take advantage of the Vierendeel effect: in fact, due to the reduced axial extensibility of the columns, all floors can be assumed subjected to the same displacement in correspondence of the removed column and, therefore, to the same internal actions. However, it should be recognised that this arrangement contradicts optimization principles [4] exclusively in favour of robustness and safety criteria. By applying these two additional criteria, 5ϕ18 reinforcing bars are arranged continuously and symmetrically in all the beams of the five floors. To respect the capacity design principles, the stirrup step becomes 7.5cm in the dissipative areas of the beams for

all the floors, whereas the stirrup diameter of all the beam-column joints increased to ϕ10 with the same step of 5cm. The other structural elements remained unchanged with respect to the *frame 1* (Fig. 4(a)). This new arrangement of the *frame 3* is depicted in Fig. 4(c).
It is important to underline that all the modifications in the arrangement of the reinforcement are verified according to the seismic codes [9],[57] and respect all the code limitations.

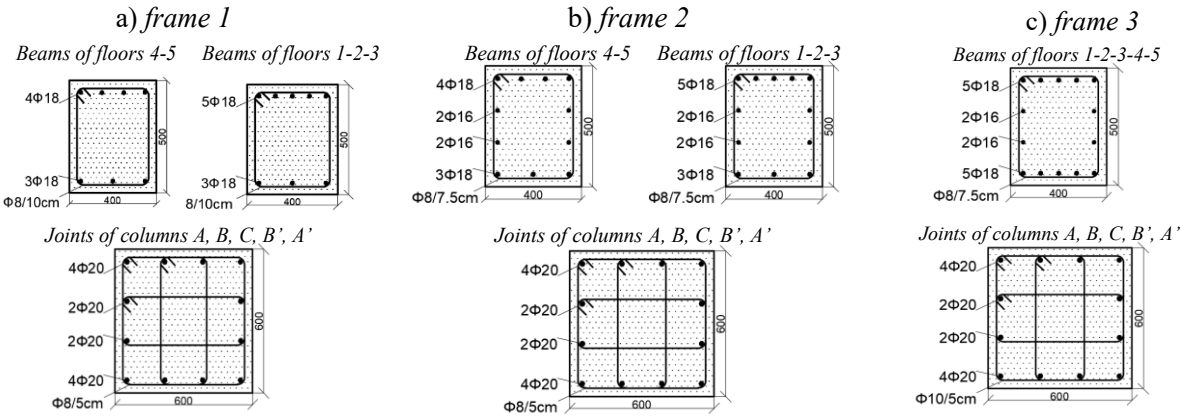

Fig. 4 Longitudinal and transverse reinforcement in the cross-sections of the beams of Fig. 3(a) and in the beam-column joints for: (a) *frame 1*; (b) *frame 2;* (c) *frame 3*. The dimensions are in millimetres if not indicated.

4. FE MODELS OF THE 2D RC MR FRAMES WITH THE COLLAPSE SCENARIO

The FE models of the three entire frames have been defined adopting the FEM software ATENA 2D [56]. All the assumptions (i.e., typology and size of the mesh, mesh elements, constitutive laws of materials, number of iterations, tolerances, boundary conditions) [58]-[67] behind the numerical modelling have been validated by reproducing the results in terms of load-deflection curve and horizontal-vertical displacement curve of the experimental test in [68], on a beam-column subassembly with similar characteristics of the frame under study, as explained in Appendix A. The only differences concern the material properties and geometrical characteristics, while the remaining assumptions and modelling strategies are the same, as summarized in Table 1.

Table 1. Modelling assumptions explained in Appendix A.

Equilibrium of forces	- System of equations solved using the standard Newton-Raphson iterative procedure with "line search" - Max iteration limit: 2500 - Convergence criteria: 1.0% for the norm of displacement error; from 1.0% to 2.5% for the norm of residual force error; from 1.0% to 2.5% for the maximum error of residual forces; 1.0‰ for the out-of-balance energy error
Kinematic compatibility	- Macro-elements modeled as plane stress quadrilateral isoparametric finite elements, based on linear polynomial interpolation, with 4 Gauss integration points - Mesh size ranging between 5 and 10 cm. - Longitudinal and transverse reinforcement modelled by discrete approach
Constitutive relationships	- *Concrete compression behaviour*: curvilinear response with linear compression softening (LCS) - *Concrete tensile behaviour*: bi-linear law with elastic response until tensile strength and post peak linear tension softening (LTS), calibrated for ultimate strain at zero stress equal to 10 times the strain of the peak tensile strength - *Cracking*: smeared crack modelling with fixed crack model - *Reinforcement*: bilinear constitutive model with hardening law for both compression and tension

The compressive behaviour of concrete is shown in Fig. 5(a)-(b)-(c), respectively, for the *frame 1*, *frame 2* and *frame 3* considering the mean values of the mechanical properties, while the tensile behaviour is shown in Fig. 5(d). As it can be observed, the constitutive model in compression has

been derived for: unconfined concrete (i.e., effective concrete cover - "unconfined"), confined concrete in non-dissipative areas of beams ("beam ND"), confined concrete in dissipative area of beams ("beam D" considering the step of the stirrups), confined concrete in columns, confined concrete in beam-column joints (considering the stirrup diameter). The adoption of a constitutive law accounting for confinement effects also in beams is extensively justified in Appendix A and derives from the arching compressive forces that arise in the beams during the initial stages (i.e., flexural and softening response [40]) of the progressive collapse phenomena.

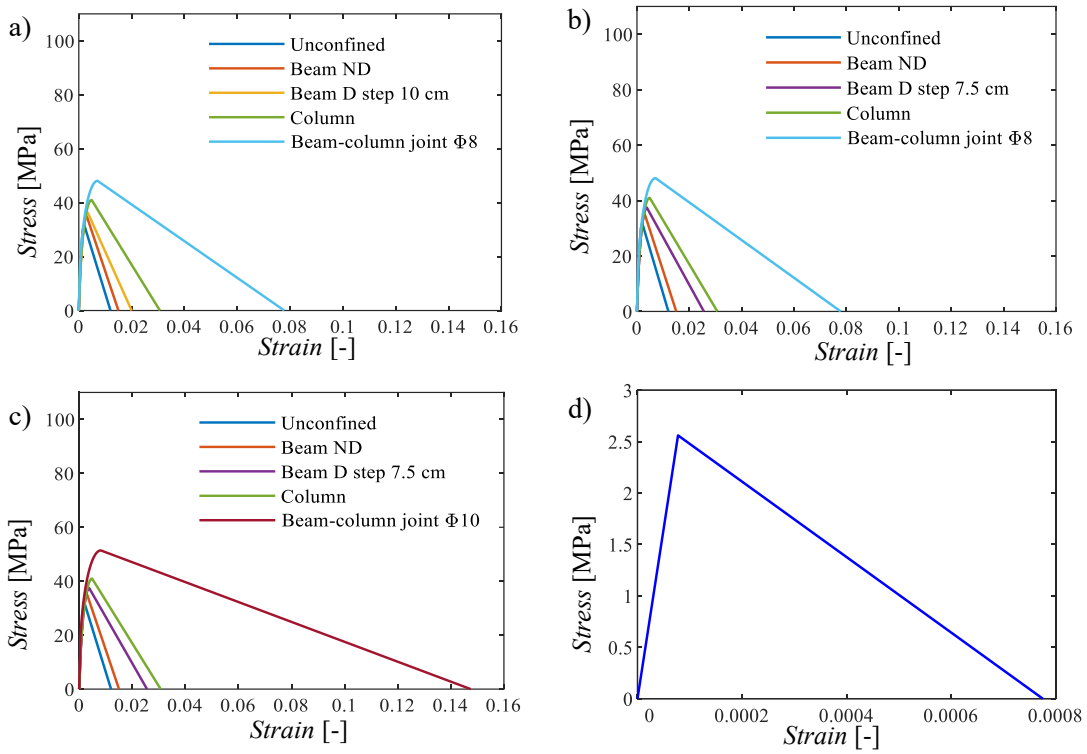

Fig. 5 Constitutive laws: concrete compressive behaviour, respectively, for the *frame 1* (a) *frame 2* (b) and *frame 3* (c); (d) concrete tensile behaviour for all the frames and elements. Mean values of mechanical properties are assumed.

The compressive and tensile behaviour of steel is shown in Fig. 6 considering the mean values of the mechanical properties.

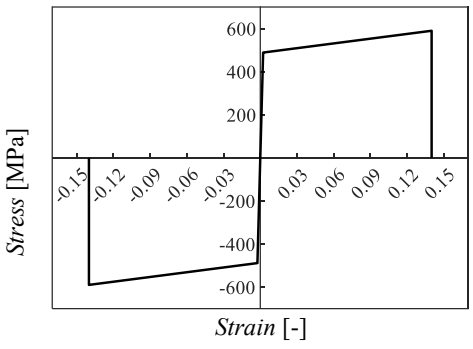

Fig. 6 Constitutive law for the steel in tension and in compression for all the frames and for both stirrups and longitudinal reinforcement, assuming mean values of mechanical properties.

More details about the statistical values of the mechanical properties for both the materials are clarified in the following section.

The boundary conditions in the FE models are defined as fully restraints at the base of the columns. As an example, the characteristics of the FE models in terms of joints, lines, macro-elements and reinforcement discrete elements are shown in Fig. 7 for the *frame 1*, depicting also the failure scenario.

The failure scenario of the central supporting column belonging to the internal frame (Fig. 2(a)) has been selected since it is not influenced by the infills located along the orthogonal perimeter frames.

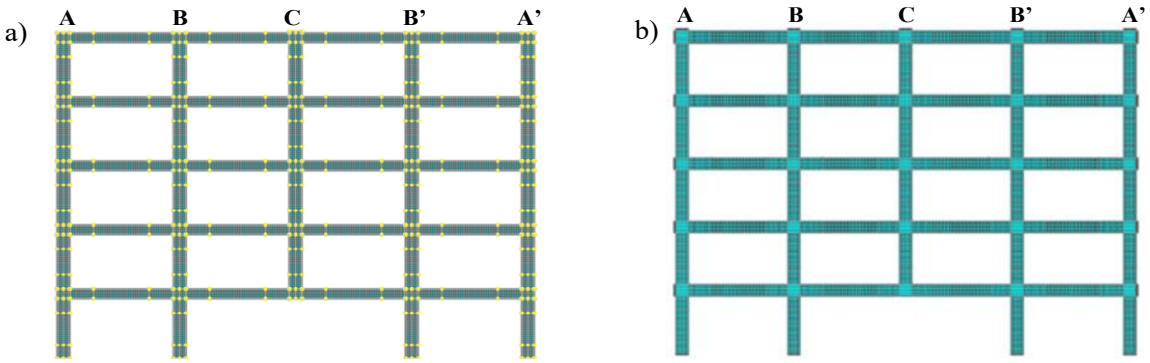

Fig. 7 Representation of the 2D entire frame in the FEM software, for example, regarding the *frame 1*: (a) joints, lines, macro-elements and mesh; (b) longitudinal and transverse reinforcement.

4.1 Contribution of the orthogonal framed systems

With the aim to include 3D effects in the 2D NLFE global analyses, the contribution of the orthogonal systems to the frames under study is modelled, in a simplified way, by means of equivalent elastic springs. In fact, in a 3D structure, the constraints due to the transverse frames (i.e., in the y-z plane of Fig. 2) surely enhance the robustness by stiffening the frame in the x-z plane [27],[69]-[74]. The transverse beams belonging to the orthogonal frames and slabs with one-way joists, have been herein modelled, in a straightforward manner, by means of equivalent elastic translational springs. The rotational stiffness has not been considered [69],[75] since it has a negligible influence on the flexural response without any influence on the development of catenary action. The stiffnesses of these translational elastic springs are properly calibrated for each joint of the five floors (apart from the ones of the column involved in the failure scenario) through elastic analyses in SAP2000 [76] conducted on the 3D structure, in absence of the central supporting column (Fig. 8(a)). Specifically, the elastic axial (diaphragm) contribution of the one-way RC slabs having thickness of 4cm [9]-[10] with the one-way joists of 20cm is modelled. The orthogonal frames (in the y-z plane) are assumed to have the same geometrical and mechanical characteristics of the frame under study (in x-z plane). In addition, the axial and bending stiffness of beams and the bending stiffness of the columns of the frame under study (in x-z plane) are nullified since their contributions are already accounted for in the FE model, while the torsional and bending stiffness of all other beams and the bending stiffness of the other columns are reduced according to [77]-[78] to consider the cracked behaviour in a simplified way.

Table 2. Equivalent elastic springs: stiffness for each joint of the different floors.

	Spring Stiffness for column A and A' [N/m]	**Spring Stiffness for column B and B' [N/m]**
1st floor	9.775E+07	9.634E+07
2nd floor	7.143E+07	7.062E+07
3rd floor	5.291E+07	5.247E+07
4th floor	4.122E+07	4.095E+07
5th floor	3.291E+07	3.270E+07

To compute the stiffness at each joint, a unitary horizontal force in the out-of-plane direction of the orthogonal frame (i.e., x direction) is applied to that joint (Fig. 8(a)). The unitary horizontal force divided by the displacement provides the elastic stiffness of the spring at that joint. This procedure has been repeated for each joint of all the columns apart from the one subjected to the sudden collapse. It should be underlined that since the axial and bending stiffness of the beams and the bending stiffness of the column in the studied frame are nullified, the computation of the translational stiffness at one joint is not influenced by the computation at another joint. Then, a spring on each joint of the frames under study is applied in ATENA 2D considering a linear-elastic constitutive model and

assigning the spring to the centre line of the joint, as shown in Fig. 8(b). The stiffness values of these elastic springs for each joint and each floor, computed considering the mean values for concrete properties, are reported in Table 2 and are effective for all the three frames (i.e., *frame 1*, *frame 2* and *frame 3*). The order of magnitude of these stiffnesses are in line with the results in many works considering both sub-assemblies and frames [69],[75],[79].

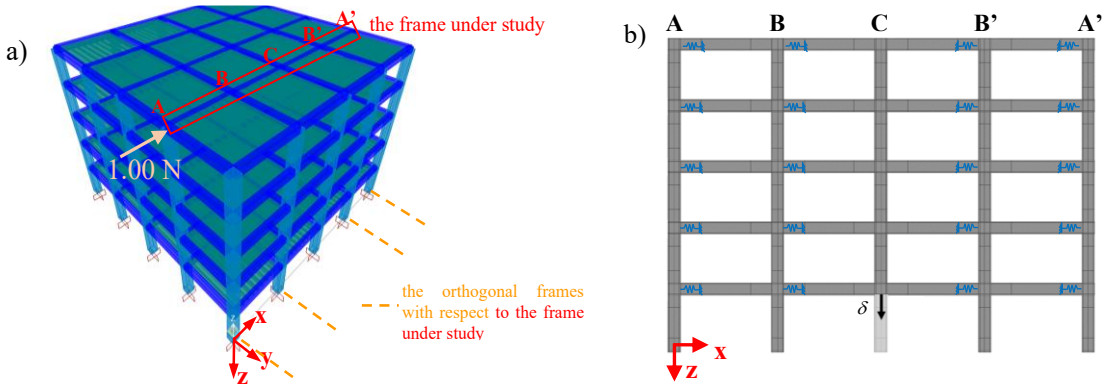

Fig. 8 Calibration of the lateral springs: (a) example of calibrating the spring stiffness for the last floor, column A, in SAP2000; (b) springs (in blue) applied to the frames under study in ATENA-2D.

5. PROBABILISTIC SAMPLING

A full probabilistic approach has been performed, by sampling the following basic random variables regarding both materials and loads: concrete compressive strength f_c; reinforced concrete specific-weight ρ; reinforcing steel elastic modulus E_s; reinforcing steel yielding strength f_y; reinforcing steel ultimate strength f_u; reinforcing steel ultimate strain ε_{su}; permanent structural load G_1; permanent non-structural load G_2; floor variable load Q_f; roofing variable load Q_r and snow load Q_s. According to the first step of the procedure (Section 2), the LHS technique [41] has been adopted to sample 100 realizations. A sample size of 100 is assumed in line with the "rule of thumb" for which the sampling size should be around 10 times of the number of basic variables in order to have a reliable evaluation of the output variables [41]. At the same time, a sensitivity analysis of the final results as a function of the sampling size has been performed demonstrating the effectiveness of this size: the final probabilistic results have been evaluated for increasing discrete values of the sampling size and showed a quite stable trend in correspondence of 100 sampled values.

Table 3. Summary of the sampled basic random variables.

	Distribution	*Mean value*	*Coefficient of variation [-]*
f_c	Lognormal [44]	31.9 *MPa* [7],[9]-[10]	0.15 [44]
ρ	Normal [45]-[46]	25 *kN/m*^{3} [7],[9]-[10]	0.05 [45]-[46]
E_s	Lognormal [44]	210000 *MPa* [7],[9]-[10]	0.03 [44]
f_y	Lognormal [44]	488.6 *MPa* [7],[9]-[10]	0.05 [44]
f_u	Lognormal [44]	589.8 *MPa* [7],[9]-[10]	0.05 [44]
ε_{su}	Lognormal [44]	0.14 [79]-[83]	0.09 [44]
G_1	Normal [43]	16 *kN/m* [7],[9]-[10]	0.05 [43]
G_2	Normal [43]	13 *kN/m* [7],[9]-[10]	0.05 [43]
Q_f	Gumbel [43]	7.3 *kN/m* [42]	0.20 [45]-[46]
Q_r	Gumbel [43]	1.8 *kN/m* [42]	0.20 [45]-[46]
Q_s	Gumbel [43]	4.7 *kN/m* [42]	0.20 [45]-[46]

Mean values and coefficients of variation (CoVs) of the random variables concerning the material properties as well as the CoVs of the loads have been taken in accordance to [42]-[46]. Instead, as for the mean values of the latter ones, the nominal values deriving from the analysis of the effective area have been assumed for the permanent loads [7],[9]-[10], whereas the mean values for the variable loads have been obtained from the characteristic ones, related to a reference period of 50 years [42].

Even if there is not a mandatory regulation, Model Code 2020 [84] suggests for the variable loads an annual reference period in case of an accidental scenario condition. However, the assumption of a reference period of 50 years for the variable loads is in line with other hazards, like seismic one, assumed in the design of the frames under investigation within a multi-risk view. Moreover, the larger the reference period the more severe is the load intensity and, thus, this hypothesis is on safe side.

Table 4. Full correlation matrix.

	f_c	ρ	E_s	f_y	f_u	ε_{su}	G_1	G_2	Q_f	Q_r
f_c	1	0	0	0	0	0	0	0	0	0
ρ		1	0	0	0	0	0	0	0	0
E_s			1	0	0	0	0	0	0	0
f_y				1	0.85	-0.50	0	0	0	0
f_u					1	-0.55	0	0	0	0
ε_{su}						1	0	0	0	0
G_1			_				1	0	0	0
G_2								1	0	0
Q_f									1	0
Q_r										1

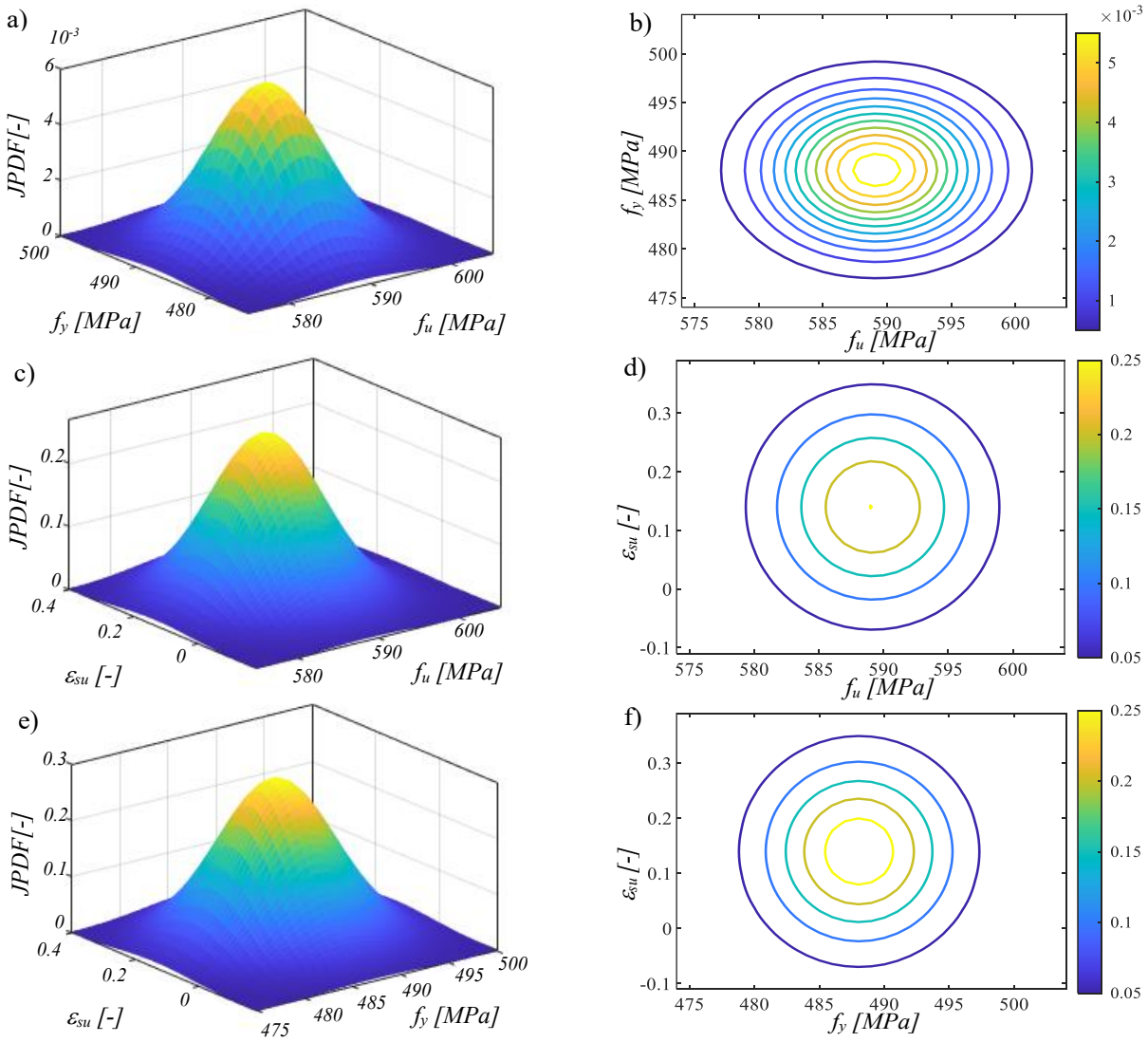

Fig. 9 a) JPDFs and contour plots for the following sets of correlated random variables: a)-b) f_u and f_y; c)-d) f_u and ε_{su}; e)-f) f_y and ε_{su}.

Regarding steel inelastic properties, a mean value for the ultimate strain equal to 0.14 with a ratio between the ultimate and yielding strength equal to 1.21 are assumed. These assumptions are in accordance with different experimental tests investigating the robustness of RC sub-assemblies [68],[79]-[82] as well as in line with the results of monotonic tensile tests conducted on a wide range of steel reinforcing specimens [83].

As highlighted in Subsection 4.1, the equivalent elastic springs have been calibrated adopting the mean properties of concrete parameters. The aleatory properties of the springs for each one of the 100 random simulations have been obtained by multiplying their values by the quantity E_{ci}/E_{cm}, where E_{cm} is the mean concrete elastic modulus and E_{ci} is the concrete elastic modulus corresponding to the i^{th} sample of the concrete compressive strength. Table 3 resumes all the information regarding the distributions of the random variables with the corresponding mean values and CoVs.

The LHS realizations strictly depend on the correlation between the variables. In the case under analysis, correlations exist between the following variables: the tensile yielding strength f_y, tensile ultimate strength f_u and tensile ultimate strain ε_{su} of the reinforcement steel. The values suggested by [44] are used for the correlation coefficients. The full correlation matrix is reported in Table 4. In Fig. 9, the joint probability density functions (JPDFs) together with the contour plots for the three correlated variables are shown.

For completeness, it should be highlighted that this probabilistic analysis does not include geometrical uncertainties for their reduced influence on the global structural resistance [44],[59]-[62].

6. PROBABILISTIC CAPACITY CURVES TO ASSESS THE ENERGY-BASED DAFs

This section deals with the computation of both the aleatory capacity curves and DAFs according to the second and third step of the procedure in Section 2. These steps are needed to perform probabilistic static-equivalent NLFE global analyses accounting for the dynamicity of the column removal scenario.

The DAFs are computed applying the energy equivalence method proposed by Izzuddin [23]. This method is based on the idea that an accidental column loss is a phenomenon physically associated to a sudden application of gravity loads on the affected sub-structure, i.e., the spans above. At the beginning (i.e., at the instant of column failure) the gravity load is larger than the static structural resistance, which determines an increase in the deformations and, consequentially, in the associated kinetic energy. While deformations grow more and more, the static structural resistance increases as well, causing a reduction in the kinetic energy, i.e., in the velocities. The maximum dynamic displacement δ_d is reached when its derivative is zero, thus, when the kinetic energy is null. This coincides with the performance point where the external work W, i.e., the work done by the gravity loads, is equal to the internal energy U, which is the energy absorbed by the structure. The internal energy can be computed as the area under the capacity curve (i.e., $P(\delta)$). These two quantities (i.e., W and U) can be computed for the i^{th} realization, as follows:

$$W = \lambda_d P_0 \delta_d \tag{2}$$

$$U = \int_0^{\delta_d} P(\delta) d\delta \tag{3}$$

The performance point where the two curves (i.e., internal energy curve and external work curve) have the intersection, corresponds to the dynamic displacement δ_d, as Fig. 10(a) illustrates for one aleatory case of the *frame 2*. Then, the dynamic load $P_d=\lambda_d P_o$ is evaluated as the load corresponding to the dynamic displacement in the pushdown curve (as shown in Fig. 10 (b)). Finally, the DAF, denoted as λ_d, can be computed according to Eq.(4) [23], where P_o represents the static gravity concentrated force at the top of the removed column.

$$\lambda_d = \frac{P_d}{P_o} \tag{4}$$

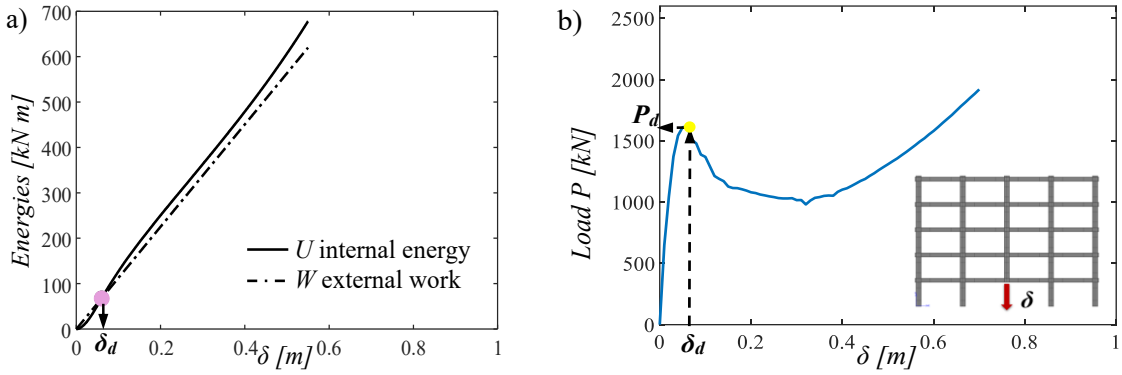

Fig. 10 Example of application of the energy equivalence method on a realization of the *frame 2*: (a) energy curves and calculation of the dynamic displacement; (b) pushdown curve with the calculation of the dynamic load.

In the following, the probabilistic characterization of the two quantities P_o and P_d as well as of the energy-based DAFs are illustrated.

6.1 Assessment of the static gravity load P_o

For the calculation of the DAFs λ_d related to any aleatory frame, the static gravity concentrated force at the top of the removed column P_o needs to be evaluated. Since all the applied loads derive from a probabilistic sampling, the force P_o is consequentially a random variable. In detail, it has been computed multiplying the 100 aleatory distributed gravitational loads per unit meter (i.e., permanent structural and non-structural loads, snow load and live loads - distinguishing between the floors and the roof), placed according to the load combination of [8], by the effective width to obtain the corresponding resultant gravity force in the point of column removal. The aleatory values of P_o are shown in Fig. 11. It should be noted that these values of P_o are equal for all the three frames since they basically depend on the sampled external loads, which are equal for all the three frames (i.e., *frame 1*, *frame 2* and *frame 3*).

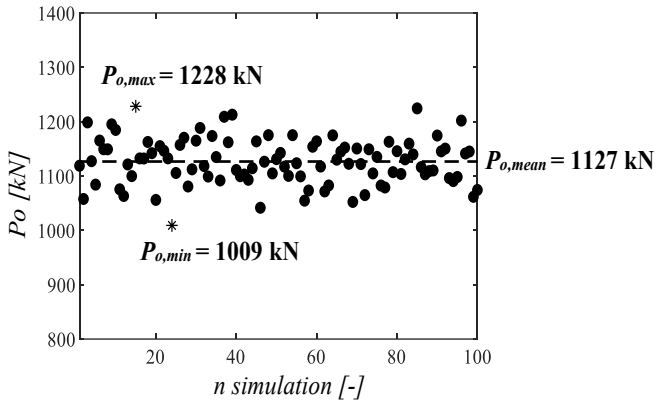

Fig. 11 Aleatory values of the static gravity concentrated force at the top of the removed column for the three frames.

6.2 Aleatory capacity curves and assessment of the dynamic response P_d

To obtain the capacity curves, needed for the evaluation of the dynamic response P_d, static displacement-controlled pushdown NLFEAs have been performed [85]-[87] for the entire frames, as the second step of the procedure (Section 2). Three sets of 100 random NLFE models have been defined, each one with different values for the material properties but having the same geometry, restrains and constraints. For these analyses, the entire frames have been modelled without the central supporting column. Each numerical simulation consists in imposing an increasing vertical displacement δ with increase of 1cm where the column is accidentally removed and monitoring the reaction in the same point. The application of such gradually increasing displacement determines a continuously changing stress path in the entire structure. The results of these NLFE global analyses are aleatory force-displacement curves, the so-called aleatory pushdown or capacity curves.

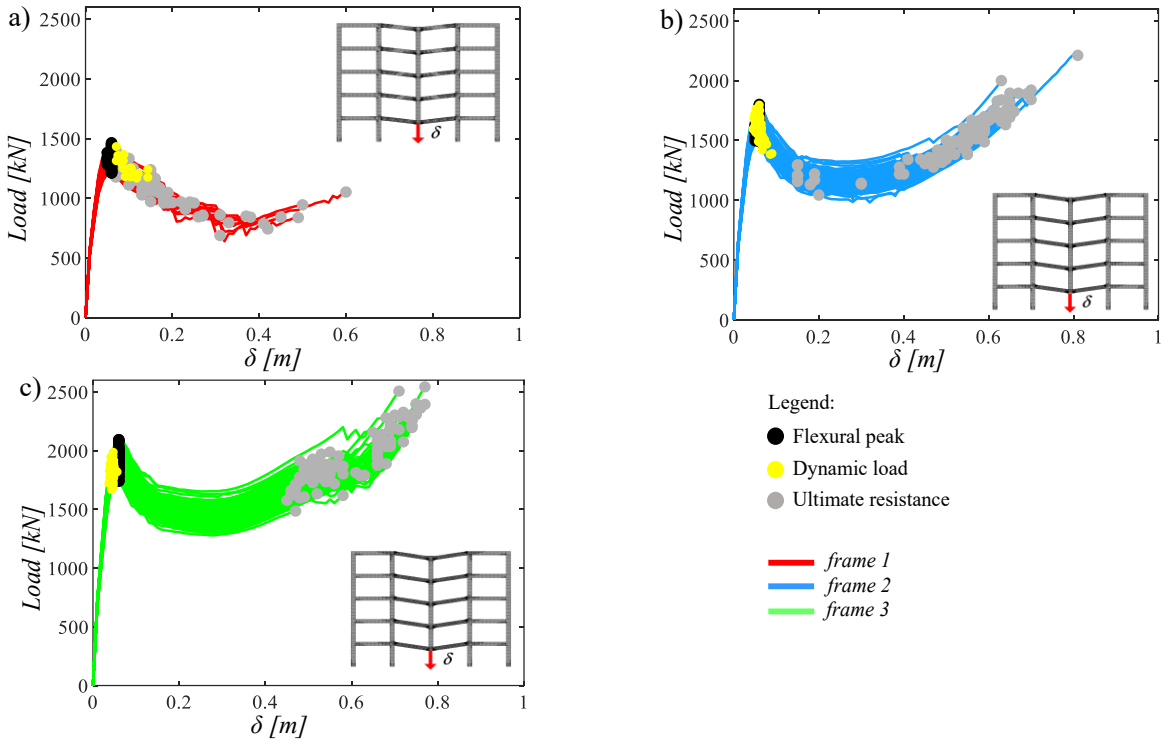

Fig. 12 Aleatory capacity curves considering flexural peak (black dots), ultimate resistance (grey dots) and the resistance at the energetic equivalence (yellow dots): (a) *frame 1*; (b) *frame 2*; (c) *frame 3*.

In Fig. 12, the 300 aleatory capacity curves related to the three RC MR frames (i.e., *frame 1*, *frame 2* and *frame 3*) are showed, highlighting the maximum resistant load in the flexural phase or flexural peak $P_{MAX,FL}$ (black dots), the ultimate resistance before failure $P_{MAX,RES}$ (grey dots) and the resistance at which the energetic equivalence is reached P_d (yellow dots). In addition, an example of an aleatory failure mode for each one of the three frames is shown. From the simulations, especially, of the *frame 2* and *3*, three different stages can be clearly visible: flexural stage including compressive arch action, softening stage and catenary effect stage [40]. The first one is initially governed by a linear elastic behaviour of the materials until $P_{MAX,FL}$ is reached. For all the three frames, the displacements needed to reach $P_{MAX,FL}$ are similar but the values of the corresponding peak loads change. This is mainly due to the differences in the reinforcement layouts as well as to the dispersion of concrete compressive strength, which also influences the behaviour of the transverse elements as defined in Subsection 4.1, since the steel yielding strength is characterized by a quite low CoV (i.e., 0.05). After the flexural peak, the softening stage follows, characterised by a reduction of the reaction due to the crushing of concrete and consequent reduction of compression behaviour of the beams for the constraints (i.e., the surrounding columns). The amplitude of the second stage, is more varying as a function of the sampled material properties. The third stage starts when the catenary effect activates, determining an increase of the reaction for increasing vertical displacements in the point of the removal. This effect derives from a combination of both the flexural and catenary effects in the reinforcing bars and, thus, is mainly governed by the steel properties (e.g., CoV associated to the steel ultimate strain, i.e., 0.09). Consequently, also the displacement value, at which the catenary peaks are reached, varies as well. By comparing the three frames, it is more and more evident that the catenary is activated thanks to the reinforcement continuity and starts for low displacements around 0.2 m thanks to the side face rebars [40]. Moreover, the catenary effects (i.e., recovery in resistance) is evident in both the *frame 2* and *frame 3* but it is quite completely absent in the *frame 1*, confirming the effectiveness of the robustness improvements. This absence is due to concrete crushing in the softening stage as well as failure in longitudinal rebars (without the help of the side fare rebars), as investigated in terms of strain results in the next sections.

By applying the energy equivalence approach in all 300 aleatory frames, the external works and internal energies are evaluated, as previously described, and then, the aleatory dynamic displacements

δ_d with corresponding dynamic loads P_d are computed. In Fig. 12, the resistances at which the energy equivalence is reached (i.e., yellow dots) are also indicated. The equivalences are obtained for lower imposed vertical displacement for both the *frame 2* and *frame 3* with respect to the *frame 1*. This last result highlights that not very large strains in the reinforcement are demanded at the performance points (i.e., yellow dots) and, also confirms the simplified assumption of the equivalent elastic springs since the horizontal displacements corresponding to performance points (i.e., yellow dots) are not too large [40]. It should also be underlined that in Fig. 12(a) for the *frame 1* only the P_d values, related to the cases in which energy equivalences are reached, are shown. The aleatory dynamic loads are shown in Fig. 13 for the three frames. It should be highlighted that for the *frame 1* (Fig. 13(a)) (i.e., designed according to current standards) the two energy curves do not find an intersection in majority of the cases, meaning that the structure, in these cases, is not able to sustain the accidental loss of the central supporting column. For this reason, in Fig. 13(a) the aleatory dynamic reactions are represented only for the cases where the energy equivalences were reached: these points are close to the flexural peaks. In addition, the *frame 3* leads to the largest values of dynamic reactions if compared to the *frame 2*. This is because the larger quantity of reinforcement implies a larger bearing capacity for the RC structure.

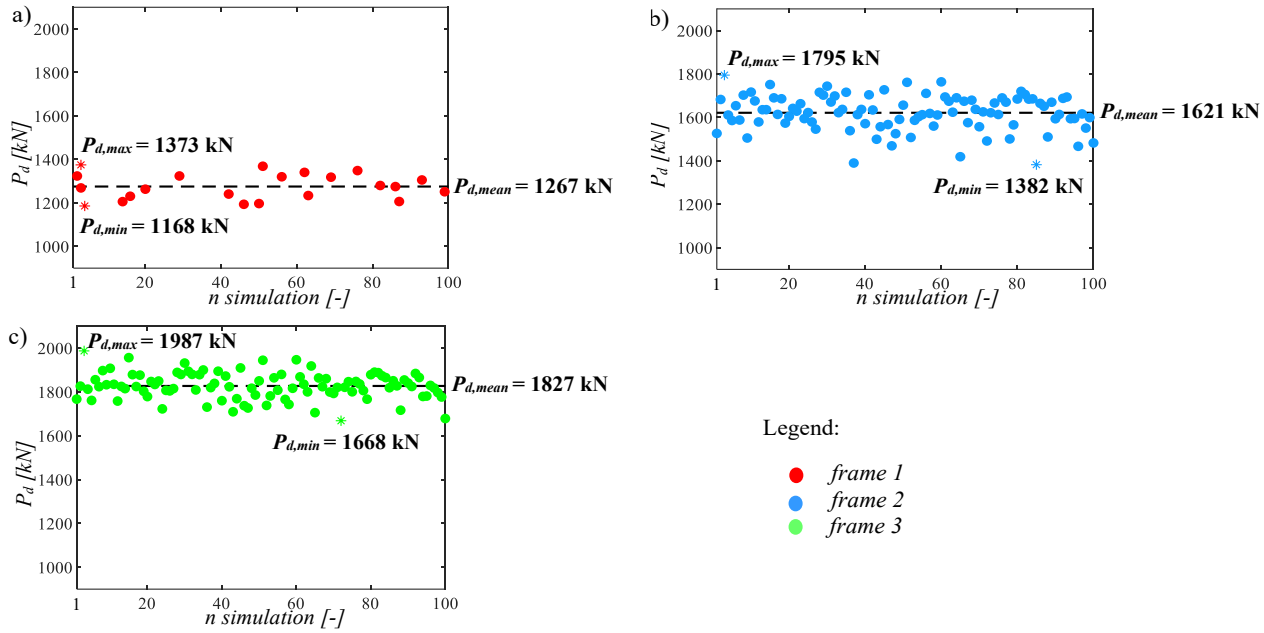

Fig. 13 Aleatory dynamic gravity load P_d obtained from the capacity curves for: (a) *frame 1* (considering only cases with energetic equivalence); (b) *frame 2*; (c) *frame 3*.

6.3 Assessment of the aleatory Dynamic Amplification Factors (DAFs)

As described in the previous subsection, once the aleatory concentrated dynamic load is computed as the value of the capacity curve corresponding to the dynamic displacement, the corresponding aleatory energy-based DAF can be computed as $\lambda_d = P_d / P_o$ through Eq.(4), and represents the third step of the procedure in Section 2. Fig. 14 shows the aleatory values of the DAFs as a function of the number of simulations (from 1 to 100) for each frame. It should be noted that the larger the capacity of the structure to sustain the accidental event, the larger is the DAF to be applied to gravity loads. For this reason, the mean value of the DAFs for the *frame 3*, equal to 1.62, is larger than the one for the *frame 2*, equal to 1.44. Again, for the *frame 1* only the cases corresponding to energy equivalences are shown, with a mean value of 1.16, confirming the trend previously explained.

From these results, it is interesting to note that the aleatory DAFs in case of non-linear response are lower than 2.0, value indicated by [20]-[21] for linear static analyses. Similar results may be found in different experimental and numerical investigations [88]-[89].

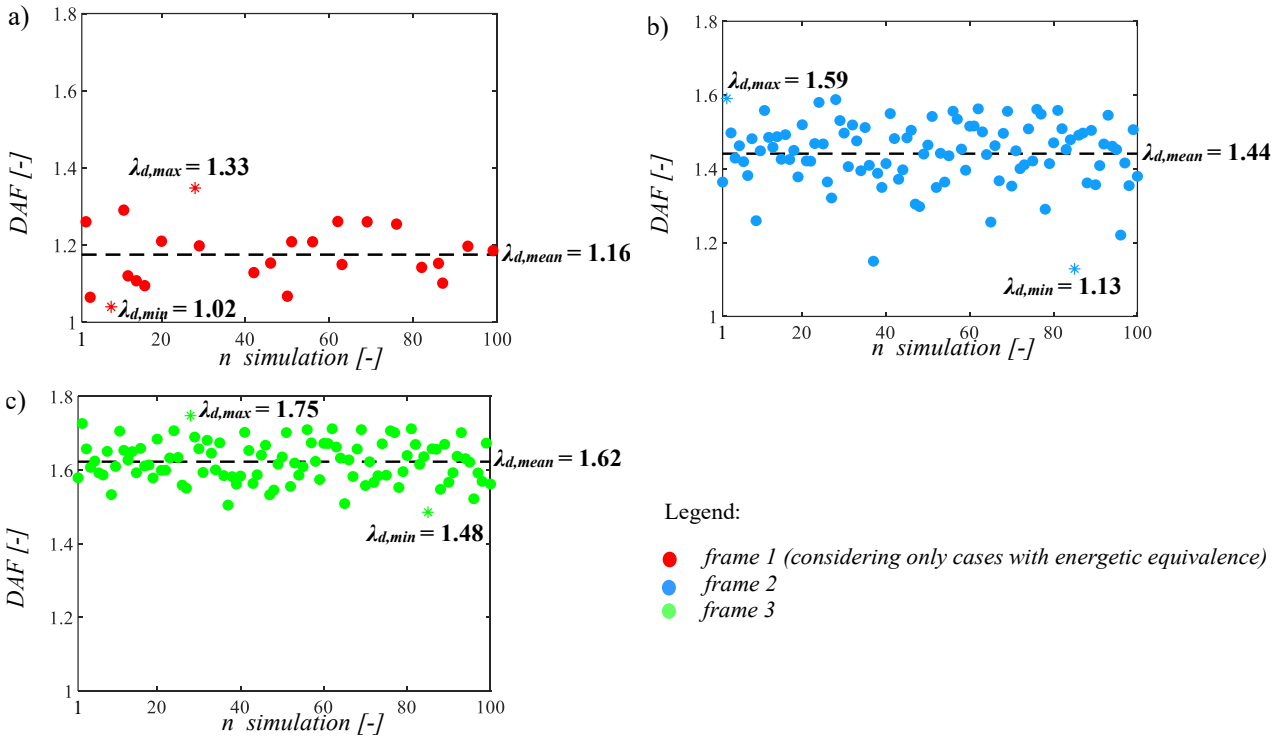

Fig. 14 Aleatory energy-based DAFs for: a) *frame 1*; b) *frame 2*; c) *frame 3*.

7. PROBABILISTIC ANALYSES FOR THE RELIABILITY ASSESSMENT OF THE STRUCTURAL ROBUSTNESS

In the first subsection, the probabilistic static-equivalent NLFE global analyses are described, and the results are probabilistically modelled by means of appropriate probability density functions (PDFs). In the second subsection, the cumulative distribution functions (CDFs) related to the ultimate capacity of the different materials as well as the failure probabilities are computed to achieve the reliability assessment of the robustness at structural level with respect to the ULS for the three frames under investigation (i.e., *frame 1*, *frame 2* and *frame 3*). A discussion of the results is in the last subsection.

7.1 Probabilistic analysis: aleatory static-equivalent NLFE simulations

In compliance with the fourth step of the procedure (Section 2), for both the *frame 2* and *frame 3*, two sets of 100 static-equivalent NLFE global simulations have been performed by applying the gravity loads placed in line with the accidental load combination of [8] (the same adopted in Subsection 6.1), removing the central supporting column and amplifying the gravity loads only on the spans of the five floors adjacent to the central column through the previously computed DAFs. The other spans are not amplified since the propagation of the dynamic effects is damped by the structural RC elements, as achieved in some preliminary dynamic simulations and in accordance with [39],[88]-[89]. After the amplification, collapse was never reached in all the simulations confirming the prediction of the energetic approach. As for the *frame 1*, similarly, static-equivalent NLFE global simulations have been carried out when the DAFs exist, whereas, in the other cases, static-equivalent NLFE global simulations have been run achieving two possible results as predicted by the energetic approach: i) failure reached after removing the supporting column without amplifying the loads; ii) failure reached by slightly amplifying the loads after the removal. These results, in terms of collapse or no-collapse related to the three frames, also confirm that the simplification of applying a concentrated displacement instead of a distributed configuration (hypothesis closer to the reality) in the evaluation of both capacity curves and energetic performance points is a reasonable hypothesis.

Then, for each set of simulations, the aleatory peak principal total strains (ε) in significant points of the entire RC frames (Fig. 15(a)-(b), Fig. 16(a)-(b), Fig. 17(a)-(b)) have been extrapolated at the last

numerical step of equilibrium. In detail, the points of both beams and columns close to each beam-column joint have been considered, identifying four sections for each beam-column joint (except for the corner columns as well as for the last floor where three or two cross-sections are, respectively, present). Successively, in each cross-section, different points have been considered distinguishing between the points of the confined concrete core, of the upper and lower longitudinal reinforcement, of the side face rebars (only for the *frame 2* and *frame 3*) and of the stirrups. For clearness, it is worth noting that the colours adopted in Fig. 15 - Fig. 17 to distinguish between the different materials are the same of the constitutive laws shown in Fig. 5, with different characteristics.

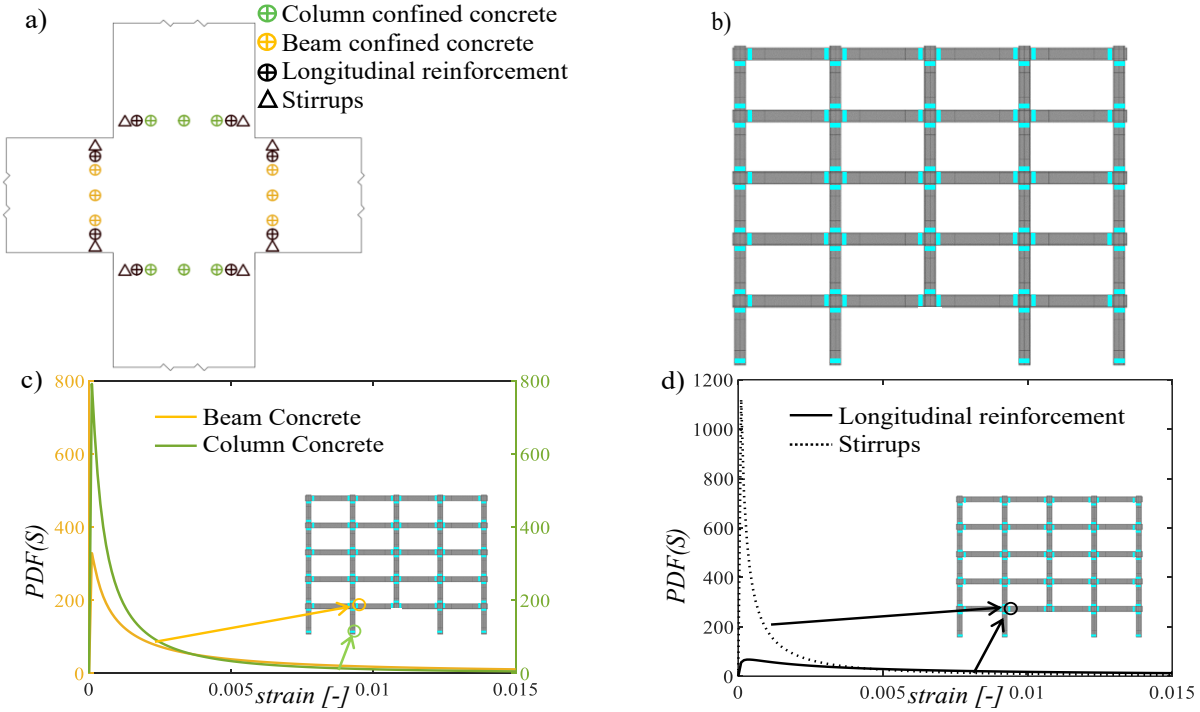

Fig. 15 *Frame 1*: a)-b) Cross-sections close to the beam-column joint where the demand is evaluated; c)-d) PDFs of the demanded aleatory peak strains in the most stressed cross-sections for each material.

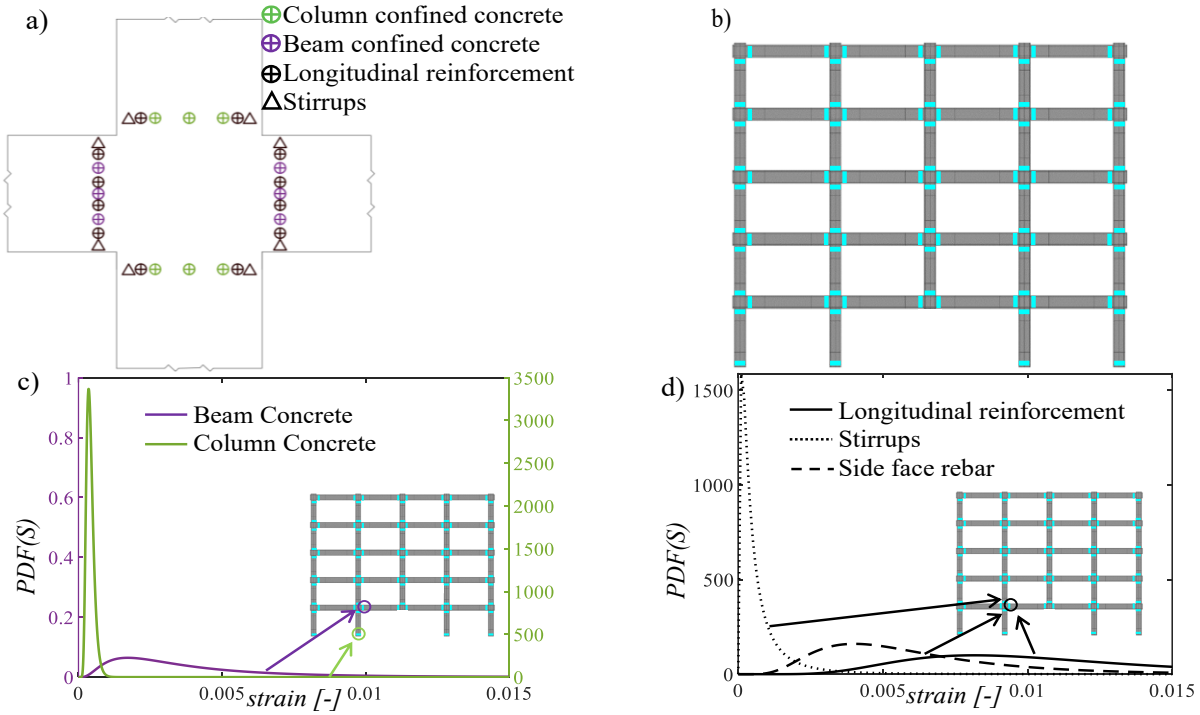

Fig. 16 *Frame 2*: a)-b) Cross-sections close to the beam-column joint where the demand is evaluated; c)-d) PDFs of the demanded aleatory peak strains in the most stressed cross-sections for each material.

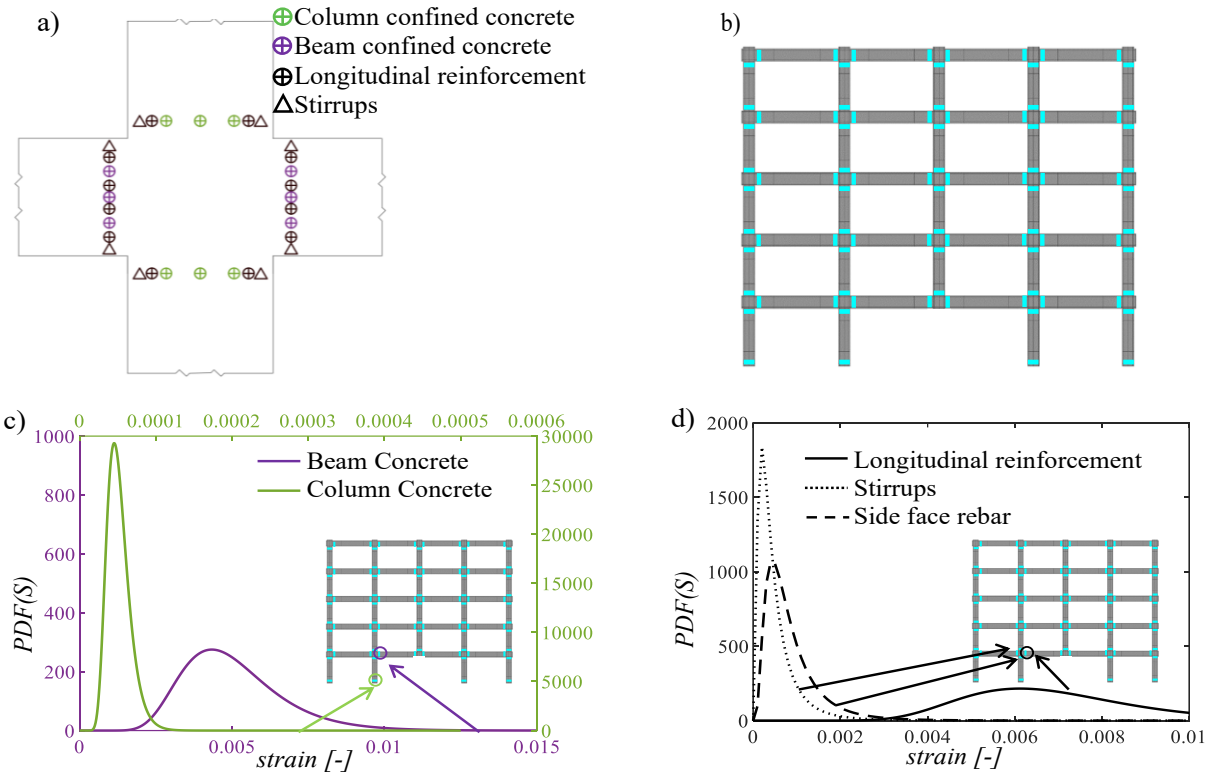

Fig. 17 *Frame 3*: a)-b) Cross-sections close to the beam-column joint where the demand is evaluated; c)-d) PDFs of the demanded aleatory peak strains in the most stressed cross-sections for each material.

A statistical inference analysis was needed to investigate the PDFs for the aleatory peak strains in the different points of the structure by applying both the Chi-Square and Anderson Darling tests. In detail, the Chi-Square goodness of fit test is adopted to check whether the frequency distribution of a variable (i.e., the strain) is different from the expectation, while the Anderson Darling test is used to verify, with a certain level of significance (i.e., 5%), if a sample of data comes from a population with a specific distribution. Hence, the lognormal distribution has been selected as the proper probabilistic distribution since it has always passed the goodness of fit test with a high p-values (around 0.8). The statistical inference analysis has been performed for all the three frames leading to the same conclusions. In this way, the statistics of the output aleatory peak strains have been computed through the Maximum Likelihood technique [90] including also the statistical uncertainties according to the Fisher Information Matrix [91] due to the no very large size, especially, for the *frame 1*. Fig. 15(c)-(d), Fig. 16(c)-(d), Fig. 17(c)-(d) show examples of the PDFs of the demanded aleatory peak strains in the most stressed points for each material or component (i.e., confined concrete in beams, confined concrete in columns, longitudinal reinforcing bars, side face rebars and stirrups) related to the *frame 1*, *frame 2* and *frame 3*, respectively.

7.2 Reliability assessment

According to the last step of the procedure in Section 2, for each material of structural elements (shown in Fig. 5), denoting as S the demand (i.e., the aleatory peak strains monitored at the points) and C the capacity (i.e., the aleatory ultimate strain of the materials), the failure probability is the probability that the aleatory demand overcomes the aleatory capacity with respect to the ULS, thus it can be expressed through the convolution integral [49] as follows:

$$p_f = P(C < S) = \int_0^\infty \left[\int_0^s f_C(c)\,dc \right] f_S(s)\,ds = \int_0^\infty F_C(s) f_S(s)\,ds \tag{5}$$

where $F_C(s)$ is the CDF of C evaluated at specific realizations of the demand (i.e., s), $f_S(s)$ and $f_C(c)$ are the PDFs, respectively, of S and C.

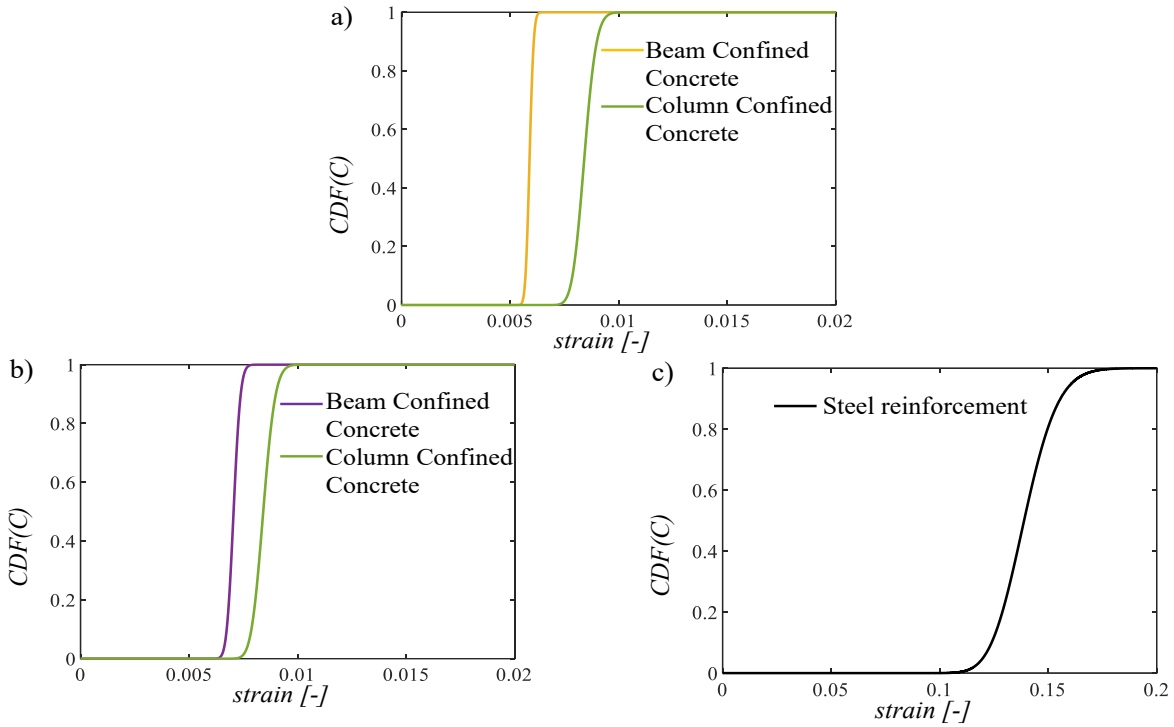

Fig. 18 CDFs of the capacity for different materials: a) confined concrete in the most stressed cross-section for the *frame 1*; b) confined concrete in the most stressed cross-section for both the *frame 2* and *frame 3*; c) steel reinforcement.

For each of the points in any cross-section of the beam-column joints within each frame, a convolution integral is performed between the PDF of the demand $f_S(s)$, computed in the previous subsection, and the CDF of the capacity $F_C(s)$, obtained as the CDF of the sampled ultimate strains thresholds (Fig. 18). In detail, for the steel, the ultimate strain is considered, as sampled in Section 5, while for the concrete, the ultimate strain in confined condition, as confirmed by the numerical analyses, is indirectly computed from the sampled concrete compressive strength, and assumed equal to the strain corresponding to a post-peak strength equal to the 85% of the peak strength, on safe side. All the ultimate strains are modelled through lognormal distributions, as described in Section 5. For example, Fig. 18(a)-(b) show the CDFs of the capacity for confined concrete related to the *frame 1*, *frame 2* and *frame 3*, respectively. Fig. 18(c) shows the CDF of the capacity for steel, that is equal for any reinforcement and for all three frames.

The probabilities, computed through Eq. (5), represent the failure probabilities with respect to the ULS, correspond to the term $P[C|LD]$ of Eq. (1) and are related to a system failure condition since NLFE global analyses have been carried out.

In Fig. 15(c)-(d), Fig. 16(c)-(d), Fig. 17(c)-(d), the PDFs of the demand S in the most stressed sections are shown for the different materials and, respectively, for the *frame 1, frame 2* and *frame 3*. It should be underlined that the concrete in tension is not considered for computation of the failure probabilities since it does not behave as a resisting material in the failure modes at those deformation levels.

Note that regarding the *frame 1*, the total probability theorem [92] has been adopted to compute the failure probabilities of the beams and columns in the spans close to the failure scenario due to the collapses of the majority cases achieved from the probabilistic static-equivalent NLFE global simulations. The expression [92] applies, as follows:

$$p_{f,frame1} = \frac{N_{non-collapse}}{N_{tot}} \cdot \left[\int_0^{\infty} F_C(s) f_S(s)\, ds \right]_{non-collapse\ cases} + \frac{N_{collapse}}{N_{tot}} \cdot 1 \qquad (6)$$

where, $N_{collapse}$ is the number of collapse cases derived from the energy equivalence approach, N_{tot} is the total number of samples (i.e., 100) and $N_{non\text{-}collapse}$ is the complementary part of $N_{collapse}$ with respect to N_{tot}.

In the following, the failure probabilities for each section close to the beam-column joints are shown, separating the probability related to a) the confined concrete material (only in compression), b) the longitudinal reinforcement and c) the transverse reinforcement for the *frame 1* (Fig. 19), *frame 2* (Fig. 20) and *frame 3* (Fig. 21), respectively. This probabilistic computation in the most stressed points allows also to define the propagation of the damage, useful for robustness considerations.

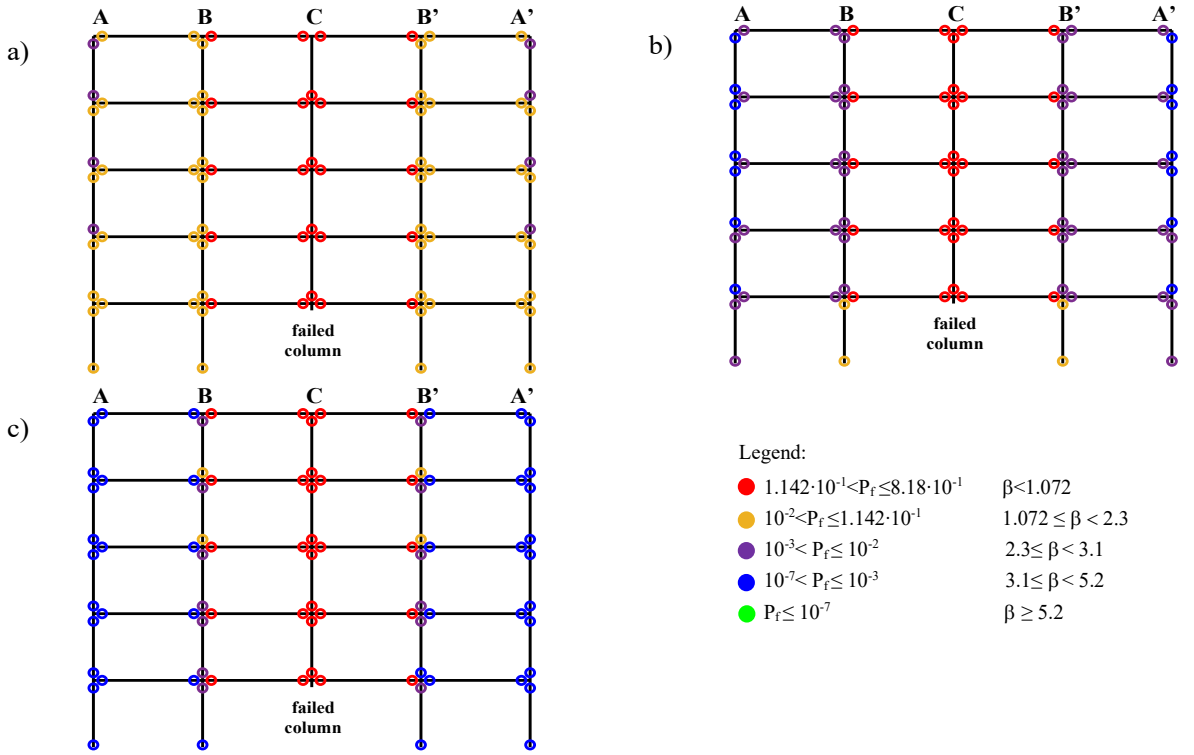

Fig. 19 Failure probabilities for the *frame 1* considering: a) confined concrete; b) steel longitudinal reinforcement; c) steel transverse reinforcement.

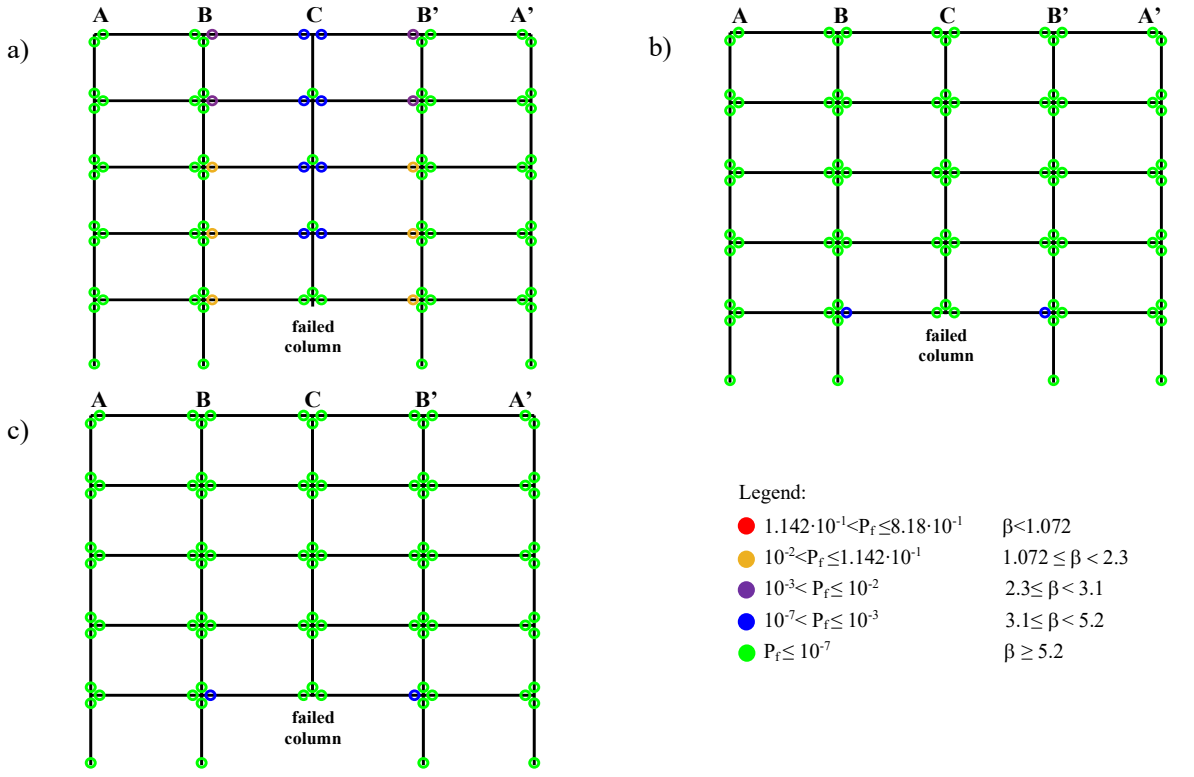

Fig. 20 Failure probabilities for the *frame 2* considering: a) confined concrete; b) steel longitudinal reinforcement; c) steel transverse reinforcement.

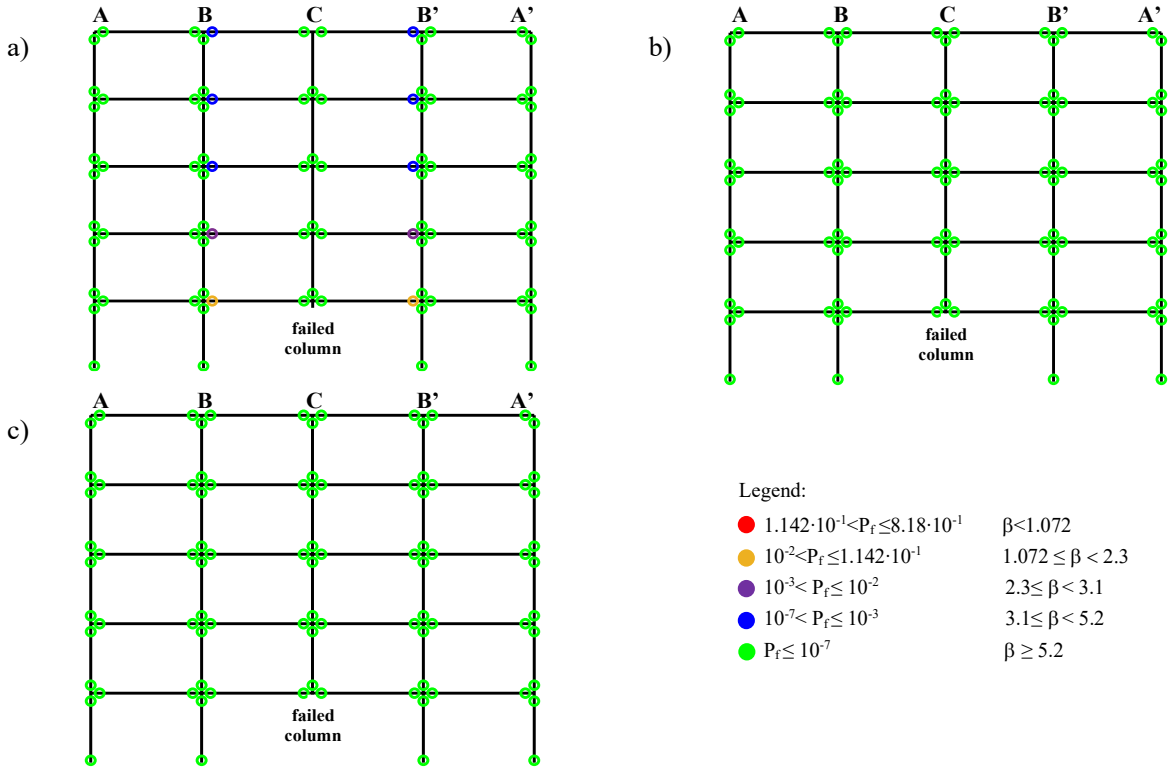

Fig. 21 Failure probabilities for the *frame 3* considering: a) confined concrete; b) steel longitudinal reinforcement; c) steel transverse reinforcement.

Regarding, especially, the *frame 2* and *frame 3*, in the beams close to the failed column, the failure probabilities at the concrete level decrease in the upper stories in the cross-sections connected to the columns B and B' as well as are higher than those related to the cross-sections connected to the column C. This is due to the constrain actions, higher at the lower levels, developed by the other structural members. In Fig. 20(a), it is possible to observe that the cross-sections connected to the column C at the first floor show low failure probabilities but slightly higher than those corresponding to upper floors. This happens numerically also in the *frame 1* (Fig. 19(a)) and *frame 3* (Fig. 21(a)) and it is a consequence of the absence of the failed column at the first floor.

As a general observation, the *frame 1* is characterized by the largest failure probabilities if compared to the other two *frames* and this is valid for all the investigated materials. In fact, the *frame 1* shows failure probabilities in concrete (Fig. 19(a)) between 10^{-3}-10^{-1} in the lateral spans, even if they are indirectly affected by the column loss. The largest value (i.e., 0.818) is obviously reached in the beams of the first floor adjacent to the removal, but also the beams of the upper floors are subjected to values much larger than 10^{-1}. Regarding the longitudinal reinforcement (Fig. 19(b)), the failure probabilities are lower in the external spans but are always larger in the central ones (i.e., much larger than 10^{-1}). This suggests that the amount of reinforcement, derived from the standard seismic design, is not enough to guarantee resistance in robustness response. In addition, since the stirrups (Fig. 19(c)) are not subjected to the same state of stress as for the longitudinal reinforcement, the failure probabilities are lower.

By analysing the results of the *frame 2*, important improvements are registered, especially, regarding the failure probabilities for the longitudinal reinforcement (Fig. 20(b)). Apart from the beams of the central spans at the first floor, all the other beam-column sections are characterized by very low failure probabilities (i.e., lower than 10^{-7}). This result suggests the importance of considering the side face rebars in the design of this type of structures. Regarding the confined concrete in compression (Fig. 20(a)), lower failure probabilities are obtained with respect to the previous case, especially, in the external spans, confirming that the presence of the side face rebars tend to reduce the mechanical effort at the concrete level. In fact, the safety level regarding confined concrete in terms of β minimum (in 50 years as structural reference period) is far below 1 for the *frame 1*, while it has a value larger

than 1 for the *frame 2* (i.e., 1.08). Similar considerations can be drawn for the *frame 3* (Fig. 21), with the main difference that concrete is characterized by even lower failure probabilities with respect to the previous case (i.e., β minimum equal to 1.23). The values of β higher than 1 for the *frame 2* and *frame 3* represent an important achievement in line with the provisions recommended in [14] (i.e., 1.5) where the structural reference period is 1 year.

Regarding the steel longitudinal reinforcement, the β minimum is far below 1 for the *frame 1*, equal to 5.11 and 7.45 for, respectively, the *frame 2* and *frame 3*. These last two results become slightly lower (i.e., up to around 4) even if the mean value of the ultimate strain of the reinforcement is assumed lower than 0.14 (e.g., up to 0.075 [9]) since the energetic equivalences are reached for not large vertical displacements (Section 6.2).

It is necessary to highlight that these very low failure probabilities at the reinforcement level (Fig. 20(b) and Fig. 21(b)) together with the activation of catenary effect visible in Fig. 12(b)-(c) are of great importance especially when dynamic phenomena and large displacement are involved and, thus, the response is mainly governed by the steel.

The maximum failure probabilities obtained in this investigation (i.e., 0.82, 0.14, 0.11 for, respectively, the *frame 1*, *frame 2* and *frame 3*) are comparable with the ones in different studies. For instance, in [34], considering an amplification of the load equal to 1.3, failure probabilities of around 0.75 for complete damage limit state were obtained for seismically designed 2D RC internal frames, in case of lateral column failure scenario. The frames were characterised by continuous and symmetric longitudinal reinforcement, equal in all the floors. However, in [34], a lower CoV (i.e., equal to 0.1) for the concrete strength was adopted. Another comparison can be carried out with respect to [38], where a force-based reliability computation is considered and a failure probability of 0.074 for a five-storey RC frame is obtained, in case of central supporting column loss scenario. The frame of [38] is a seismically-designed symmetric frame and the beams have continuity with a comparable longitudinal reinforcement layout between the lower and upper chords in all the floors. However, it should be underlined that in [38] a force-based approach instead of a strain-based one has been adopted and the steel properties are characterised by a lower dispersion in the statistical characterization. Finally, with reference to the results by [39], planar frames (both internal and perimetral) of two RC office buildings are studied in terms of failure probability, and values of 0.173 and 0.254 were obtained for, respectively, the 3-story and 6-story internal frame. However, the buildings have horizontal stiffness provided by the bracings and no symmetry or floor equality criteria as well as no presence of side face rebars is included. In addition, a reference period for the variable loads of 5 years is assumed.

7.3 Final discussion

The proposals together with the results achieved provide the reliability levels with respect to the ULS in any structural element of the three RC MR frames having different design recommendations with respect to robustness. From the comparison between the three RC MR frames, it is possible to observe the relevant safety advantages together with a significant reduction of the damage propagation in reliability terms when different robustness design improvements are adopted: the failure probabilities are strongly lower in the spans close to the collapse scenario, the safety level increases in any structural element for increasing distance from the collapse event highly reducing the damage propagation. In addition, the adopted robustness suggestions lead to values of β minimum slightly higher than 1 within a structural reference period of 50 years. This result is absolutely relevant since the guidelines [14] suggests a minimum value for β equal to 1.5 considering a structural reference period of 1 year. In addition, the results refer to a reference period for variable loads of 50 years differently from the suggestion in Model Code 2020 [84] of an annual reference period in case of an accidental scenario condition.

As a result, it can be concluded that for this specific failure scenario and this structural typology (i.e., cast in-situ RC structures having slabs with joists), the design with side face rebars and continuity (i.e., *frame 2*) appears to be the leading solution since it presents quite the same level of safety as the

frame 3 with reduced costs (i.e., reduced amount of reinforcement). Therefore, the design solution of the *frame 2* represents a good trade-off between principles of robustness, sustainability [1]-[3] and safety in accordance also with seismic design within a multi-risk analysis. In fact, the percentage of increase of both longitudinal and transverse reinforcement with respect to the code-conforming structure (i.e., *frame 1*) is equal to 21% for the *frame 2* and 36% for the *frame 3*.
Note also that the contribution in the global structural resistance provided by the orthogonal frame affected by the same column loss, by the infills as well as by the membrane effects are not included in the reliability analysis and, thus, the proposed results are on the safe side. Future developments of this study could investigate different failure scenarios (i.e., corner columns or second-to-last columns), also including the above-mentioned beneficial effects. In fact, the central supporting column loss is one of the most critical scenarios for the absence of the other positive effects. In addition, other load conditions combined with other structural typologies could be examined.

8. CONCLUSIONS

This study describes a strain-based 5-step procedure to assess the structural robustness in reliability terms of 2D RC MR frames located in a seismic area, in case of the accidental loss of the central supporting column. The goal was to give insights into the safety level of frames designed according to actual code rules and enhanced frames in order to achieve a more robust behaviour. In fact, actual regulations do not give any provision on the safety level to be respected in case of progressive collapse phenomena, but only recommended values are suggested. In detail, three different frames have been compared: *frame 1* designed according to the current European and Italian code rules; *frame 2* adopts continuous longitudinal reinforcement with two additional levels of side face rebars, while the *frame 3* derives from the *frame 2* adopting the same reinforcement amount in all the floors with symmetric cross-sections to exploit a global Vierendeel behaviour.
According to the 5-step procedure, a full probabilistic approach has been followed by sampling different basic random variables, related to both material properties and applied external loads.
The main outcomes can be summarized as follows:

- the results in terms of aleatory capacity curves have demonstrated how the maximum flexural capacity is found for a slightly dispersed range of the imposed vertical displacement; on the contrary, the catenary peak as well as the softening branch (including arching compressive forces) are strongly affected by all the non-linear properties of materials, leading to a strong dispersion of the results, according to the CoVs of the material properties, especially, of the ultimate strain of reinforcement steel;
- the catenary activation starts earlier when the side face rebars are added in the design and, at the same time, the resistances corresponding to the achievement of the energy equivalence are related to lower imposed vertical displacements;
- in most of the aleatory capacity curves, the *frame 1* was not able to sustain the accidental loss of the central supporting column. For these cases, the computation of the DAFs was not possible. On the other hand, the *frame 2* and *frame 3* were characterized by mean values of the DAFs equal to, respectively, 1.44 and 1.62;
- the failure probabilities are drastically reduced when the side face rebars are added into design, reducing not only the mechanical effort at the concrete level but also the failure probabilities in the longitudinal reinforcement, reaching values lower than 10^{-7};
- the frame designed according to standards (i.e., *frame 1*) presents failure probabilities of the order of 10^{-3} to 10^{-1} in the lateral spans, resulting in a spread of the damage from the central spans (directly affected by the column loss scenario) to the external spans (indirectly affected). This is not the case for the two improved solutions (i.e., *frame 2* and *frame 3*), where the lateral spans are characterised by failure probabilities lower than 10^{-7};
- the safety level in concrete in terms of β minimum is far below 1 for the *frame 1*, while it is larger than 1 in the *frame 2* (i.e., 1.08) and *frame 3* (i.e., 1.23). Regarding the longitudinal reinforcement, the β minimum is far below 1 for the *frame 1*, and equal to 5.11 and 7.45 for,

respectively, the *frame 2* and *frame 3*;

- the *frame 2* appears to be the leading solution since it presents quite the same safety level of the *frame 3*, with reduced costs (i.e., additional reinforcement amount of 21% for *frame 2* and 36% for the *frame 3*).

As a general conclusion, the adopted robustness improvements always present the catenary response ensuring a stable response of the structure and lead to values of β minimum higher than 1 within a structural reference period of 50 years. This result is absolutely relevant and on safe side with respect to the suggestions of β minimum equal to 1.5 related to a structural reference period of 1 year and assuming a reference period for variable loads of 1 year. Therefore, especially, for cast in-situ RC structures having slabs with joists, the solution strategy of the *frame 2* represents a good trade-off between principles of robustness, sustainability and safety in accordance also with seismic design within a multi-risk analysis.

APPENDIX A

In line with the need of defining predictive numerical models in this work, a numerical model is calibrated to reproduce the results of an experimental test [68] on a beam-column subassembly extracted from a 10-story building designed in Seismic Category D according to ACI 318 Building Code [93]. The experimental test is selected since it has similar characteristics with respect to the case study of the present work. In detail, the sub-assembly (Fig. A1) is composed of two beams having a length of 5.5m and two columns of around 4.5m height. The beams have a cross-section of 71.12x50.8cm^2 and are reinforced with 2 bars of 28.65mm diameter in the lower chord and 4 or 2 bars of 25.4mm diameter in the upper one for, respectively, dissipative and non-dissipative area. The dissipative area has a length of 1.83m. The transverse reinforcement is composed of 2-leg stirrups having 12.7mm diameter with a step of 22.8cm or 10.16cm, respectively, in non-dissipative area and dissipative area. As for the columns, their cross-section is squared and have a size of 71.12cm, while their longitudinal reinforcement is made of 12 bars of 25.4mm and the 4-leg stirrups have a step of 10.16mm and a diameter of 12.7mm.

Regarding the loading scheme, a displacement-controlled application of the load is assumed, by means of 4 hydraulic rams placed on top of the central column and imposing a rate of 25mm/minute. Four steel rods are fixed to the reaction wall to prevent any out-of-plane movement. Two concrete blocks are placed on the internal side of the upper part of the lateral columns and fixed to the reaction wall. Those concrete blocks are then connected to the column by means of 51mm steel plates constrained by four 32mm post-tensioning bars anchored to the columns themselves. The clamping force is of 2669kN. Those constraint conditions are representative of a roller-fixture (i.e., prevention of horizontal displacement). Finally, the longitudinal bars of the columns are fully embedded by two footings having width, thickness and height of 2.235x1.626x1.067m^3, respectively.

As far as concern the material properties, a campaign led to the following mean values of the mechanical properties:

- concrete compressive of 32MPa;
- concrete tensile strength of 3.1MPa;
- top bars of the beams (with diameter of 25.4mm): f_y(steel yield strength)=476MPa, f_u(steel ultimate strength)=648MPa, ε_s(ultimate strain)=0.21;
- bottom bars of the beams (with diameter of 28.65mm): f_y=462MPa, f_u=641MPa, ε_s=0.18;
- bars of the columns (with diameter of 28.65mm): f_y=483MPa, f_u=690MPa, ε_s=0.17;
- stirrups (with diameter of 10.16mm): f_y=524MPa, f_u=710MPa, ε_s=0.14.

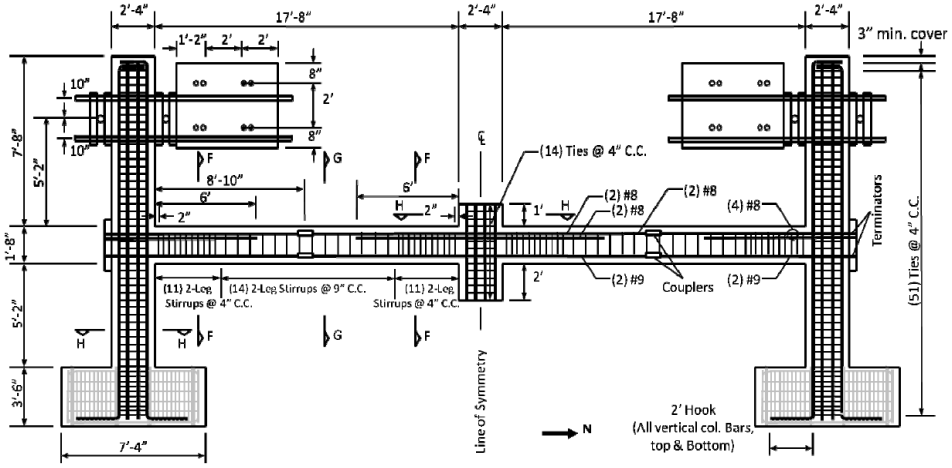

Fig. A1 Geometrical characteristics and cross-sections of the experimental test in [68] (modified from [68]).

The experimental test is reproduced in Atena 2D [56], by taking advantage of the symmetry of the problem (Fig. A2), in fact, no horizontal movements are registered in correspondence of the center line during the test. Distinction is made between concrete core and concrete cover by considering

macro-elements made of plane stress quadrilateral isoparametric finite elements, based on linear polynomial interpolation, with 4 Gauss integration points. The thickness of the macro-elements is set equal to 0.7112m for all the structural elements (i.e., beam, columns and beam-column nodes), in line with the geometrical out-of-plane dimension. The mesh size varies in the range between 0.05m and 0.10m, in line with a mesh-sensitivity analysis finalized to capture the experimental response in terms of load-deflection curve and horizontal-vertical displacement curve. The bars are considered as discrete elements.

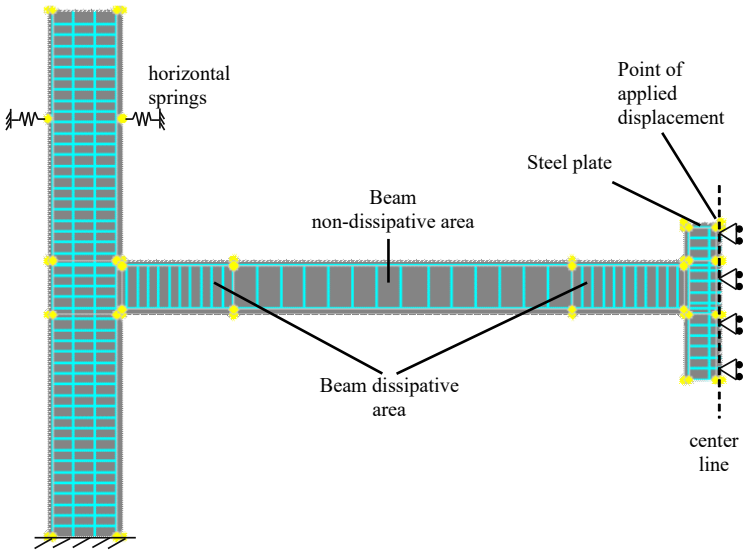

Fig. A2 Representation of the FE modeling of half of the sub-assembly: joints, macro-elements and discrete bars.

The constraint conditions are the following (Fig. A2): horizontal movements in correspondence of the center line are avoided in order to respect the symmetry of the problem; fixed horizontal and vertical movement at the base of the columns in correspondence of half of the height of the footing; two springs (with a properly calibrated stiffness of almost 140N/mm) are placed at around 30cm from the top of the column to represent the roller-fixture.

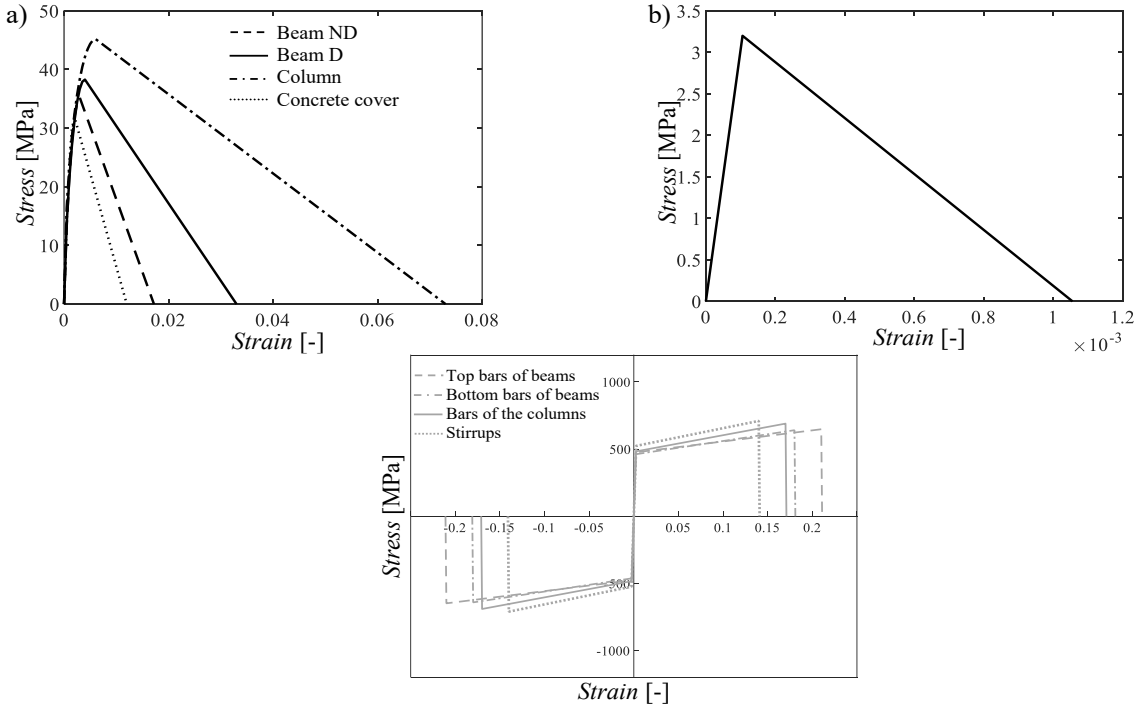

Fig. A3 Constitutive laws of materials assuming mean values of the mechanical properties for: a) concrete in compression; b) concrete in tension; c) steel bars in tension and in compression.

Concerning the concrete behaviour in compression (Fig. A3(a)), the behaviour before the peak stress is derived by the formula in CEB-FIP Model Code 90 [63], while the post-peak response is described by a linearly descending branch and it is based on a local strain softening according to Saatcioglu and Razvi model [64], in order to account for the multiaxial state of stress due to the confinement of concrete in compression. In fact, the beams are subjected to compressive forces during the initial stages of the progressive collapse phenomena, which should be taken into account both in terms of resistance and ductility. The reduction of compressive strength due to cracks is taken equal to 0.45, representing the maximal strength reduction under large transverse strain, as suggested by [65] and in line with the experimental results of 0.

The tensile concrete behaviour (Fig. A3(b)) has been modelled choosing a local strain tension softening, accounting for the tension stiffening effect [66] through a linear post-peak branch up to the zero strength in correspondence of a strain equal to $10f_{ct}/E_c$, being f_{ct} the tensile strength of concrete and E_c the secant elastic modulus, computed according to [7]. Besides, the cracking process has been reproduced using the "Smeared cracking" with the fixed crack direction model [65],[67].

As for the reinforcement steel (Fig. A3(c)), a bi-linear constitutive law in tension and in compression has been adopted with hardening law. The reinforcement has been modelled with discrete bar elements assuming a perfect bond with the surrounding concrete. It should be noted that, buckling of reinforcement in the compressive zone is not considered since no buckling phenomena were declared during the experimental test. This derives also from the seismic design with a larger number of stirrups in the dissipative zones.

Within Atena 2D [56], the loading scheme consists in the application of the self-weight, followed by an imposed vertical displacement at a rate of 1 cm in correspondence of the loading point (i.e., top of the central column). In line with the experimental test, a steel plate of around 5 cm is placed on top of the central column. The solution of the equations is solved by adopting a standard Newton-Raphson iterative procedure considering 2500 maximum iterations and respecting contemporarily all the following four tolerance criteria [58]: 1.0% for the norm of displacement error; from 1.0% to 2.5% for the norm of residual force error; from 1.0% to 2.5% for the maximum error of residual forces; 1.0‰ for the out-of-balance energy error.

The comparison between the experimental and numerical capacity curves (Fig. A4(a)) and horizontal versus vertical displacements (Fig. A4(b)) is shown. It should be underlined that not considering the concrete confinement effects implies an underestimation of both the resistance and ductility of the response with a fail in capturing the evolution of the horizontal displacements [68],[94].

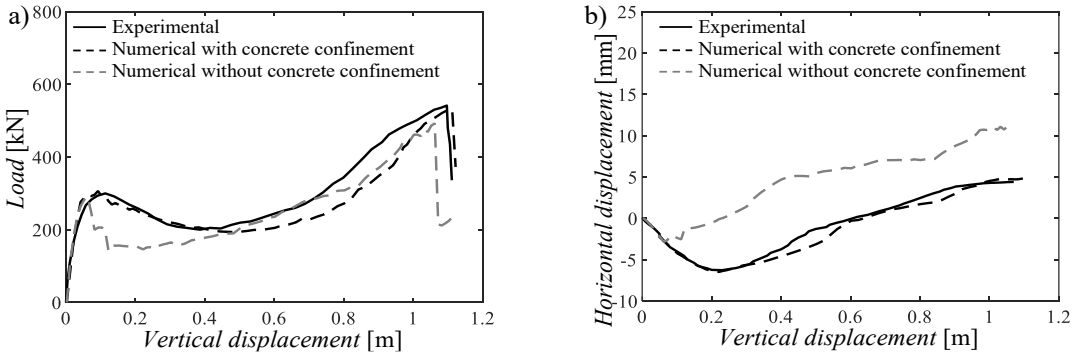

Fig. A4 Comparison between numerical and experimental response: a) capacity curve; b) horizontal displacement at the beam-column nodes.

ACNOWLEDGEMENTS

This study was carried out within the RETURN Extended Partnership and received funding from the European Union Next-GenerationEU (National Recovery and Resilience Plan-NRRP, Mission 4, Component 2, Investment 1.3—D.D. 1243 2/8/2022, PE0000005).

This work is part of the collaborative activity developed by the authors within the Commission 3 - Task Group 3.1: "*Reliability and safety evaluation: full-probabilistic and semi-probabilistic methods for existing structures*" and "*Action Group "Robustness""* of the International Federation for Structural Concrete (*fib*).

This work is also part of the collaborative activity developed by the authors within the research project "RELUIS- Costruzioni di Calcestruzzo Armato Gettate in Opera e Prefabbricate-WP11, Task 11.3 and 11.4".

This study was carried out within the Ministerial Decree no. 1062/2021 and received funding from the FSE REACT-EU - PON Ricerca e Innovazione 2014-2020. This manuscript reflects only the authors' views and opinions, neither the European Union nor the European Commission can be considered responsible for them.

REFERENCES

[1] Giacomo Caredda, Nirvan Makoond, Manuel Buitrago, Juan Sagaseta, Marios Chryssanthopoulos, Jose M. Adam, Learning from the progressive collapse of buildings, Developments in the Built Environment 15, 100194, 2023.

[2] Love, P.E.D., Matthews, J., Porter, S.R., Carey, B., Fang, W., 2023. Quality II: a new paradigm for construction. Developments in the Built Environment 16, 100261. https://doi.org/10.1016/j.dibe.2023.100261.

[3] Giacomo Caredda, Nirvan Makoond, Manuel Buitrag, Juan Sagaseta, Marios Chryssanthopoulos, Jose M. Adam, Enhancing building robustness through a fuse-based, Developments in the Built Environment segmentation framework 19, 100515, 2024.

[4] Zeng Menga, Zhuohui Zhanga, Dequan Zhangc, Dixiong Yangb, An active learning method combining Kriging and accelerated chaotic single loop approach (AK-ACSLA) for reliability-based design optimization, Comput. Methods Appl. Mech. Engrg. 357 (2019) 112570.

[5] Castaldo, P., Amendola, G., Giordano, L., Miceli, E., Seismic reliability assessment of isolated multi-span continuous deck bridges, Ingegneria Sismica, 2022, 39(3), pp. 26–51

[6] Akhavan Kazemi, M., Hoseini Vaez, S. R., & Fathali, M. A. (2022). An eco-friendly reliability-based design optimization of intermediate reinforced concrete moment frames. European Journal of Environmental and Civil Engineering, 27(5), 1876–1896.

[7] European Committee for Standardization, Eurocode - Basis of structural and geotechnical design, 1990.

[8] European Committee for Standardization, Eurocode 1 - Actions on structures - Part 1-7: General actions - Accidental actions, 1991.

[9] NTC2018, Technical Standards of Construction 2018, DM 17.01.18, Ministry of Infrastructures, Update February 2018.

[10] MIT, Istruzioni per l'applicazione dell'«Aggiornamento delle "Norme tecniche per le costruzioni"» di cui al decreto ministeriale 17 gennaio 2018., 2019.

[11] *fib*, Model Code for Concrete Structures, 2010.

[12] General Services Administration (GSA). Progressive collapse analysis and design guidelines. Washington, DC: Office of Chief Architects; 2003.

[13] Department of Communities and Local Government. The building regulations 2010 - structure: approved document A. UK: HM Government; 2010.
[14] CNR, Istruzioni per la valutazione della robustezza delle costruzioni, 2018.
[15] ASCE Standard 7-02, Minimum Design Loads for Buildings and Other Structures (ASCE 7-16) (2016), American Society of Civil Engineers, Reston, VA.
[16] Australian Building Codes Board (ABCB). National construction code (NCC). Council of Australian Governments; 2016.
[17] China Association for Engineering Construction Standardization (CECS). Code for anti-collapse design of building structures, CECS 392: 2014. Beijing (China); 2014.
[18] Ellingwood BR. Mitigating risk from abnormal loads and progressive collapse. J. Perform. Constr. Facil. 2006;20(4):315–323.
[19] F. Biondini, "A Measure of Lifetime Structural Robustness," in *Structures Congress 2009*, 2009, pp. 1–9, doi: 10.1061/41031(341)193.
[20] GSA, alternative pathanalysis and design guidelines for progressive collapse resistance, 2013.
[21] Department of Defense USA, design of buildings to resist progressive collapse, 2016.
[22] J. M. Adam, F. Parisi, J. Sagaseta, and X. Lu, "Research and practice on progressive collapse and robustness of building structures in the 21st century," *Eng. Struct.*, 173, 122–149, 2018.
[23] B. A. Izzuddin, A. G. Vlassis, A. Y. Elghazouli, and D. A. Nethercot, "Progressive collapse of multi-storey buildings due to sudden column loss - Part I: Simplified assessment framework," *Eng. Struct.*, vol. 30, no. 5, pp. 1308–1318, 2008, doi: 10.1016/j.engstruct.2007.07.011.
[24] E. A. Shalva Marjanishvili, "Comparison of Various Procedures for Progressive Collapse Analysis," *Journal of Performance of Constructed Facilities,* p. 365–374, 2006.
[25] T. Kim, J. Kim, and J. Park, "Investigation of progressive collapse-resisting capability of steel moment frames using push-down analysis," *J. Perform. Constr. Facil.*, 23(5), 327–335, 2009.
[26] V. De Biagi, F. Parisi, D. Asprone, B. Chiaia, and G. Manfredi, "Collapse resistance assessment through the implementation of progressive damage in finite element codes," *Eng. Struct.*, vol. 136, pp. 523–534, 2017, doi: 10.1016/j.engstruct.2017.01.058.
[27] B. Belletti, C. Damoni, V. Cervenka, and M. A. N. Hendriks, "Catenary action effects on the structural robustness assessment of RC slab strips subjected to shear and tensile forces," *Struct. Concr.*, vol. 17, no. 6, pp. 1003–1016, 2016, doi: 10.1002/suco.201500157.
[28] Izzuddin BA, Sio J. Rational horizontal tying force method for practical robustness design of building structures. Eng Struct. 2022; 252:113676.
[29] Colombo M, Martinelli P, di Prisco M. A design approach to evaluate the load-carrying capacity of reinforced concrete slabs considering tensile membrane action. Struct Eng Int. 2021; 31(2):260–70.
[30] Martinelli P, Colombo M, Ravasini S, Belletti B. Application of an analytical method for the design for robustness of RC flat slab buildings. Eng Struct. 2022;258:114117.
[31] Foad Kiakojouri, Valerio De Biagi, Catenary mechanism in steel columns under extreme lateral loading: A basis for building progressive collapse analysis, Developments in the Built Environment 20, 100556, 2024.
[32] JCSS. PROBABILISTIC MODEL CODE, Part 1 - BASIS OF DESIGN 2000.
[33] Botte W, Droogné D, Caspeele R. Reliability-based resistance of RC element subjected to membrane action and their sensitivity to uncertainties. Eng. Struct. 2021;238: 112259.
[34] Brunesi E, Nascimbene R, Parisi F, et al. Progressive Collapse Fragility of Reinforced Concrete Framed Structures through Incremental Dynamic Analysis. Eng. Struct. 2015;104:65-79.
[35] Arshian A, Morgenthal G, Narayanan S. Influence of modelling strategies on uncertainty propagation in the alternate path mechanism of reinforced concrete framed structures. Eng. Struct. 2016;110:36-47.
[36] Bhattacharya B. A reliability based measure of structural robustness for coherent systems. Struct. Saf. 2021;89:102050.

[37] Ding, Yang, et al. “Probabilistic Progressive Collapse Analysis of Steel-Concrete Composite Floor Systems.” *Journal of Constructional Steel Research*, vol. 129, 2017, pp. 129.
[38] Zhang, Qiang, et al. “Reliability Analysis of Reinforced Concrete Structure Against Progressive Collapse.” *Reliability Engineering & System Safety*, vol. 228, 2022, p. 108831.
[39] Droogné D, Botte W, Caspeele R. “A multilevel calculation scheme for risk-based robustness quantification of reinforced concrete frames”. Engineering Structures 160:56–70, 2018.
[40] Miceli, Elena, and Paolo Castaldo. “Robustness Improvements for 2D Reinforced Concrete Moment Resisting Frames: Parametric Study by Means of NLFE Analyses.” *Structural concrete* (2023), https://doi.org/10.1002/suco.202300443.
[41] Mckey MD, Conover WJ, Beckman RJ. “A comparison of three methods for selecting values of input variables in the analysis from a computer code”. Technometrics 21:239-45, 1979.
[42] *fib*, Partial factor methods for existing concrete structures. Bulletin no. 80., 2016.
[43] JCSS, Probabilistic Model Code, Part 2 - Load Models, 2001.
[44] JCSS, Probabilistic Model Code, Part 3 - Resistance Models, 2002.
[45] Slobbe, Arthur et al. “On the Value of a Reliability-based Nonlinear Finite Element Analysis Approach in the Assessment of Concrete Structures.” *Structural concrete : journal of the FIB* 21.1 (2020): 32–47
[46] Baravalle M, Köhler J, Sørensen JD. Calibration of partial safety factors in the Eurocodes. Table 11.Draft (02/10/2017); 2017.
[47] International Standard Organization, “ISO 2394 - General principles on reliability for structures”, 1998.
[48] ChangWu Huang, Abdelkhalak El Hami, Bouchaïb Radi Overview of Structural Reliability Analysis Methods - Part I : Local Reliability Methods; ISTE OpenScience, 2017
[49] A. Haldar and S. Mahadevan, “Probability, Reliability and Statistical Methods in Engineering Design”, *Bautechnik*, vol. 77, no. 5, May 2000.
[50] ISO 2394:2015: General principles on reliability for structures, Genéve, 2015.
[51] M. Holicky, A. Materna, G. Sedlacek, and L. Sanpaolesi, "Implementation of Eurocodes Handbook 1 - Basis of structural design. Leonardo Da Vinci Project", Garston, Watford, UK, 2004.
[52] COST TU0601 –Structural Robustness Design for Practising Engineers – Canisius, T.D.G..
[53] M.-H. Tsai and B.-H. Lin, “Dynamic amplification factor for progressive collapse resistance analysis of an RC building,” *Struct. Des. Tall Spec. Build.*, 18, no. 5, pp. 539–557, Aug. 2009.
[54] G. Xu and B. R. Ellingwood, “An energy-based partial pushdown analysis procedure for assessment of disproportionate collapse potential,” *J. Constr. Steel Res.*, 67(3), 547–555, 2011.
[55] Gino D., Miceli E., Castaldo P., Recupero A., Mancini G. “Strain-based method for assessment of global resistance safety factors for NLNAs of reinforced concrete structures”, Engineering Structures, 2024, 117625, https://doi.org/10.1016/j.engstruct.2024.117625.
[56] ATENA 2D v5. Cervenka Consulting s.r.o. . Prague. Czech Republic. 2014.
[57] European Committee for Standardization: Eurocode 8: Design of structures for earthquake resistance – Part 1: General rules, seismic actions and rules for buildings 2004.
[58] Max A.N. Hendriks and Marco A. Roosen (editors), “Guidelines for Nonlinear Finite Element Analysis of Concrete Structures”, Rijkswaterstaat Centre for Infrastructure, Report RTD:1016-1:2019, 2019.
[59] Gino, D., Castaldo, P., Giordano, L., Mancini, G., Model uncertainty in non-linear numerical analyses of slender reinforced concrete members, Structural Concrete, 2021, 22(2), 845–870.
[60] Miceli, E., Gino, D., Castaldo, P. Approaches to estimate global safety factors for reliability assessment of RC structures using non-linear numerical analyses, Engineering Structures, 2024, 311, 118193
[61] Bertagnoli, G., Ferrara, M., Miceli, E., Castaldo, P., Giordano, L. Safety assessment of an existing bridge deck subject to different damage scenarios through the global safety format ECOV, Engineering Structures, 2024, 306, 117859

[62] Ferrara, M., Gino, D., Miceli, E., Giordano, L., Malavisi, M., Bertagnoli, G. Safety assessment of existing prestressed reinforced concrete bridge decks through different approaches Structural Concrete, 2024, 25(3), pp. 1637–1657
[63] CEB-FIP Model Code 1990, First Draft, Comittee Euro-International du Beton, Bulletin d'information No. 195,196, Mars.
[64] M. Saatcioglu and S.R.Razvi, "Strength and ductility of confined concrete", J. Struct. Eng. (United States), vol. 119, no. 10, pp. 3109-3110, 1993.
[65] Vladimír Červenka, Libor Jendele, and Jan Červenka. ATENA Program Documentation Part 1 Theory. Ed. by Cervenka Consulting Ltd. 2012.
Dyngeland, T. (1989) - Behavior of Reinforced Concrete Panels, Dissertation, Trondheim University, Norway, BK-report 1989:1.
[66] Massicotte B, Elwi AE, MacGregor JG. "Tension-stiffening models for planar reinforced concrete members". Journal of Structural Engineering 116(11):3039–58, 1990.
[67] Darwin, D., Pecknold, D.A.W. (1974). Inelastic Model for Cyclic Biaxial Loading of Reinforced Concrete. Civil Engineering Studies, University of Illinois, July.
[68] Lew HS, Bao Y, Sadek F, Main JA, Pujol S, Sozen MA. "An experimental and computational study of reinforced concrete assemblies under a column removal scenario". *NIST Technical Note* 1720(106), 2011.
[69] Zheng Tan, Wei-hui Zhong, Bao Meng, Yu-hui Zheng, Shi-chao Duan, Effect of various boundary constraints on the collapse behavior of multi-story composite frames, Journal of Building Engineering, Volume 52, 2022, 104412, https://doi.org/10.1016/j.jobe.2022.104412.
[70] D. Feng, M. Zhang, E. Brunesi, F. Parisi, J. Yu, Z. Zhou, Investigation of 3D effects on dynamic progressive collapse resistance of RC structures considering slabs and infill walls, Journal of building engineering 54, 104421, 2022.
[71] Di Trapani F, Giordano L, Mancini G. Progressive Collapse Response of Reinforced Concrete Frame Structures with Masonry Infills. Journal of Engineering Mechanics 2020;146-3.
[72] Gino, D., Miceli, E., Giordano, L., Marano, G.C., Castaldo, P. Influence of Masonry Infills on Seismic Performance of an Existing RC Building Retrofitted by Means of FPS Devices, Applied Sciences (Switzerland), 2023, 13(6), 3509
[73] Belletti B, Muttoni A, Ravasini S, Vecchi F. Parametric analysis on punching shear resistance of reinforced concrete continuous slabs. Magazine of Concrete Res. 2018;71(20):1083-1096.
[74] Cantone R, Belletti B, Manelli L, Muttoni A. Compressive membrane action effects on punching strength of flat RC slabs. Key Engineering Materials 2016;711:698-705.
[75] Pham AT, Tan KH. A simplified model of catenary action in reinforced concrete frames under axially restrained conditions. Magazine of Concrete Research 2017;1700009.
[76] CSI, SAP2000 Integrated software for structural analysis and Design, Computers and Structures Inc., Berkley, California.
[77] Castaldo P, De Iuliis M. Effects of Deep Excavation on Seismic Vulnerability of Existing Reinforced Concrete Framed Structures. Soil Dynamics and Earth. Engin. 2014;64:102-112.
[78] American Society of Civil Engineers (ASCE). Pre-standard and commentary for the seismic rehabilitation of buildings, FEMA Report 356. Washington, DC; 2000.
[79] Yu J, Tan KH. Experimental and numerical investigation on progressive collapse resistance of reinforced concrete beam column sub-assemblages. Engineering Struc. 2013;55:90–106.
[80] Ren P, Li Y, Lu X, Guan H, Zhou Y. Experimental Investigation of Progressive Collapse Resistance of One-way Reinforced Concrete Beam–slab Substructures under a Middle-column-removal Scenario. Engineering Structures 2016;118:28-40.
[81] Ying Wang, Bin Zhang, Xiang-Lin Gu, Feng Lin, Experimental and numerical investigation on progressive collapse resistance of RC frame structures considering transverse beam and slab effects, Journal of Building Engineering 47, 103908, 2022.
[82] Lu X, Lin K, Li Y, Guan H, Ren P, Zhou Y. Experimental Investigation of RC Beam-slab Substructures against Progressive Collapse Subject to an Edge-column-removal Scenario 2017.

Engineering Structures;149:91-103.
[83] Caprili S, Salvatore W. Mechanical performance of steel reinforcing bars in uncorroded and corroded conditions. Data in Brief 2018;18:1677–1695.
[84] *fib*, Model Code for Concrete Structures, 2020.
[85] Marjanishvili SM. Progressive analysis procedure for progressive collapse. Journal of Performance of Constructed Facilities 2004;18(2):79–85.
[86] Khandelwal KS, El-Tawil S. Pushdown resistance as a measure of robustness in progressive collapse analysis, Engineering Structures 2011;33(9):2653–2661.
[87] Ferraioli M, Avossa AM, Mandara A. Assessment of Progressive Collapse Capacity of Earthquake-Resistant Steel Moment Frames Using Pushdown Analysis. The Open Construction and Building Technology Journal 2014;8(1):324–336.
[88] J. M. Adam, M. Buitrago, E. Bertolesi, J. Sagaseta, and J. J. Moragues, "Dynamic performance of a real-scale reinforced concrete building test under a corner-column failure scenario," *Eng. Struct.*, vol. 210, no. January, p. 110414, 2020.
[89] Zhao, Zidong, et al. "Experimental and Numerical Investigation of Dynamic Progressive Collapse of Reinforced Concrete Beam-Column Assemblies Under a Middle-Column Removal Scenario." *Structures (Oxford)*, vol. 38, 2022, pp. 979–92.
[90] Fisher RA. On an absolute criterion for fitting frequency curves. Messenger of Mathematics, 41(1): 155-160, 1912.
[91] Fisher RA. Theory of Statistical Estimation. *Mathematical Proceedings of the Cambridge Philosophical Society*. 1925;22(5):700-725. doi:10.1017/S0305004100009580.
[92] Jalayer, F., and C. A. Cornell. "Alternative Non-Linear Demand Estimation Methods for Probability-Based Seismic Assessments." *Earth. Engin. & stru. Dyn.* 38, 8 (2009): 951–972.
[93] American Concrete Institute (ACI). "Building Code Requirements for Structural Concrete (ACI 318-02)". Washington, DC, 2002.
[94] Miceli E, Ferrara S, Castaldo P, Confinement effects within the seismic design of reinforced concrete frames: reliability assessment and comparison, Engineering Structures 313, 118248, 2024 10.1016/j.engstruct.2024.118248.